Journal of Volcanology and Geothermal Research 356 (2018) 141–162

Contents lists available at ScienceDirect

Journal of Volcanology and Geothermal Research

journal homepage: www.elsevier.com/locate/jvolgeores

Counter-current convection in a volcanic conduit

A.C. Fowler[a,b,*], Marguerite Robinson[a]

[a] MACSI, University of Limerick, Limerick, Ireland
[b] OCIAM, University of Oxford, Oxford, UK

ARTICLE INFO

Article history:
Received 10 July 2017
Received in revised form 29 January 2018
Accepted 4 March 2018
Available online 9 March 2018

Keywords:
Counter-current convection
Strombolian dynamics
Two-phase flow
Flow régime transition

ABSTRACT

Volcanoes of Strombolian type are able to maintain their semi-permanent eruptive states through the constant convective recycling of magma within the conduit leading from the magma chamber. In this paper we study the form of this convection using an analytic model of degassing two-phase flow in a vertical channel. We provide solutions for the flow at small Grashof and large Prandtl numbers, and we suggest that permanent steady-state counter-current convection is only possible if an initial bubbly counter-current flow undergoes a régime transition to a churn-turbulent flow. We also suggest that the magma in the chamber must be under-pressured in order for the flow to be maintained, and that this compromises the assumed form of the flow.

1. Introduction

Strombolian volcanic eruptions (Vergniolle and Mangan, 2000) are characterised by regular explosions from the magmatic vent, in which gases are released in a rhythmic fashion. The manner of the explosions is not very violent, and the eruptions are sometimes characterised by the extreme longevity of the sequence. The type example, Stromboli, which sometimes erupts in a Strombolian eruptive style, is thought to have been erupting continuously for thousands of years.

Volcanoes which erupt in a Strombolian manner are characterised by relatively low viscosity (10^2–10^3 Pa s) gas-rich basaltic magma, and it is thought that the eruptive gases (H_2O, CO_2, SO_2 for example) are exsolved from the magma as it is depressurised on its ascent. Many examples of Strombolian-type volcanoes are known, e.g., Villarrica, Chile (Witter et al., 2004), Izu-Oshima, Japan (Kazahaya et al., 1994), Satsuma-Iwojima, Japan (Kazahaya et al., 2002), Stromboli, Italy and Mount St. Helens, United States (Stevenson and Blake, 1998). Some of these possess a lava lake at the summit of the magma column, e.g. Pu'u 'O'o, Hawaii (Witham and Llewellin, 2006), Izu-Oshima (Kazahaya et al., 1994) and Villarrica (Witter et al., 2004). Degassing phases can last from many years to millennia (Stevenson and Blake, 1998). Clearly some mechanism must be at work within the magmatic plumbing system which transports a steady supply of volcanic gases from deep below the Earth's surface to the volcanic vent.

It is generally thought that these long-lived eruptive phases are maintained by counter-current convection in the magmatic conduit which connects the magma chamber to the surface (Kazahaya et al., 1994; Stevenson and Blake, 1998; Beckett et al. 2011, 2014). The upwelling magma is bubble-rich, and this provides the buoyancy to drive the upflow. The bubbles erupt at the surface, and the degassed magma is then heavier as well as colder and more viscous, and sinks back to the chamber. As pointed out by Carrigan (1983), such counter-current convection additionally provides a mechanism to offset the heat loss to the surrounding country rock, which would otherwise cause the magma to freeze in the conduit.

There have been a number of experimental and theoretical studies of such counter-current convection. Experiments (e.g., Stevenson and Blake, 1998; Huppert and Hallworth, 2007; Beckett et al. 2011) use two liquids of differing densities and viscosities, and reveal varying flow patterns, but a core-annular flow seems to be preferred at high viscosity ratios, with the heavier more viscous fluid flowing down the outside of the pipe (Beckett et al. 2011).

This proposed mechanism of continuous passive degassing has been considered in many studies in the literature (Kazahaya et al., 1994, 2002; Shinohara et al., 1995; Stevenson and Blake, 1998; Stix, 2007; Witter et al., 2004), and more recently, direct geophysical and geochemical evidence has emerged illuminating the processes of counter-current flow (Moussallam et al., 2015; Ilanko et al., 2015; Carbone et al., 2012; Wadsworth et al., 2015). A simple model for the flow in a cylindrical conduit is analogous to the

* Corresponding author.
E-mail address: andrew.fowler@ul.ie (A.C. Fowler).

https://doi.org/10.1016/j.jvolgeores.2018.03.004
0377-0273/

two-fluid experimental studies, where bubble-rich magma ascends in the centre and heavier degassed magma descends in an outer annulus (Kazahaya et al., 1994), and the flow is driven by the density difference between the ascending and descending magmas. This pipe model has also been extended to describe convection of silicic magma in a conduit (Shinohara et al., 1995; Kazahaya et al., 2002; Stevenson and Blake, 1998). Such a model essentially treats the gas-rich and gas-poor magmas as two different fluids with different densities and viscosities. Mixing of the two magmas would be unlikely if the Reynolds number is less than 10^3 and the flow remains laminar (Shinohara et al., 1995).

Theoretical studies are in principle able to address issues which lie outside the present scope of experimental studies, in particular the rôle of convective heat transport in keeping the magma in a liquid state, and the rôle of exsolution in providing buoyancy in the central core flow, and its description as a two-phase flow. Experimental investigation of two-phase convection in the conduit is challenging. The heat transfer issue can perhaps be ignored, but in order for exsolution to occur due to pressure release, a large pressure drop is necessary; at a laboratory scale, this suggests enormous velocities, which mitigates against the attainment of laminar flow. A way round this is for the liquid to have very high viscosity, and probably much higher than basaltic magma, in view of the laboratory length scale. For materials such as golden syrup this requires cold temperatures, and the issue of having dissolved gas becomes an issue; but the attainment and maintenance of large pressure drops seem hazardous.

There have been a number of numerical studies of two-phase flow in a volcanic conduit related to the present investigation. Melnik (2000) provides a homogeneous model of bubbly flow, with application to explosive eruptions. Starostin et al. (2005) also presented a two-phase flow model for explosive eruptions, assuming homogeneous flow (i.e., with a single velocity). Bercovici and Michaut (2010) presented a full two-fluid two-phase flow model, but were concerned with unidirectional flows and the transition to supersonic flow. Others (Burton et al., 2007; Witham, 2011) consider two-phase flow in the context of Strombolian eruptions, but there appears not to have been a corresponding two-phase model of the corresponding counter-current flow. The physics of exsolving two-phase flows has been discussed by Gonnermann and Manga (2012), who also summarise recent modelling efforts. James et al. (2008) discuss models of slug flow in a volcanic context. Mangan et al. (2004) consider bubble nucleation in some detail, but their two-phase flow model is quite simple. Pioli et al. (2012) provide experimental results, and are particularly focussed on régime transition. Sparks (2003) summarises much of the two-phase flow theory that was developed around the time of the eruption of the Soufrière Hills Volcano, Montserrat (Voight et al., 1999), in the late 1990s, for example by Melnik and Sparks (1999), Barmin et al. (2002), Massol and Jaupart (1999), and Melnik and Sparks (2002); he also draws attention to a parallel Russian literature, most of it in Russian, but adequately summarised by Slezin (2003). Some of these models are fairly simplistic, and all of them are concerned with unidirectional flow, and are derived from the earlier work by Vergniolle and Jaupart (1986) on separated flow and Vergniolle and Jaupart (1990) on foams. The situation is reviewed by Vergniolle and Gaudemer (2015), who re-iterate the difficulty associated with analysing the counter-current two-phase flow in a Strombolian conduit.

Burton et al. (2007) draw attention to the likelihood of régime transition in Strombolian conduits, and specifically from bubbly to slug flow, and this effect will form a central theme to our paper. Jaupart and Vergniolle (1988, 1989) conceived of what is usually taken to be an alternative explanation for the bubbly flow in the conduit. In their model, exsolution occurs in the underlying chamber, forming a foam at the chamber roof. This provides the source of the gas bubbles in the conduit.

In this paper we re-examine the question of modelling magma flow in a conduit, in which volatiles are exsolved and thus drive a permanent buoyancy-induced counter-current convective flow. We frame our model in the context of a two-phase bubbly flow, which we are then able to simplify to a form which is essentially capable of analytic solution. As discussed above, there has been a lot of two-phase flow modelling for unidirectional flows, and while it has been contemplated for counter-current flows (Vergniolle and Gaudemer, 2015), no such model appears to have been proposed: this paper addresses that omission. We identify a parametric limit which ensures fully-developed flow, and show that it is only physically appropriate for sufficiently long conduits, or sufficiently viscous magma, and we are then able to draw specific conclusions on the pressure and bubble fraction profiles in the conduit.

It is fairly evident during eruptions that the bubbly flow style is not maintained to the outlet vent of the conduit; for example, the occurrence of mild explosions (Strombolian 'burps'), or more violent ejections of gas and ash (Carbone et al., 2012) are indicative of churn or slug-type flow, but in the context of a theoretical model, it is not obvious how or why this should occur. Régime transitions have been studied experimentally, but there is little understanding of what causes them to occur. In this paper, we shall find that régime transition is an essential component in modelling the counter-current flow.

As we shall see, in our conception, there is no significant difference between the conceptual picture of Jaupart and Vergniolle and that considered here of exsolution in the conduit: the only difference is quantitative, and concerns what the initial bubble volume fraction is at the base of the conduit.

2. A model for two-phase flow in a conduit

In this section we study a model of counter-current dispersed two-phase convection in a conduit; initially this will be taken to be a two-dimensional channel, but later the model will be applied to a cylindrical conduit, or pipe. The flow is driven by the buoyancy created by volatile exsolution as the magma ascends. As we have explained above, our primary motivation lies in extending earlier theoretical studies to a more realistic situation where two-phase exsolving counter-current flows are considered. But it should be emphasised that this description falls short of realism in several regards. Firstly, it is obviously an idealisation to consider a conduit with straight-sided walls (firstly, a channel, and subsequently, a pipe). Irregular flow geometries may in themselves render the theory inadvisable, particularly as to whether a core-annular flow is relevant. Perhaps more importantly, as emphasised by Sparks (2003), exsolution changes the liquidus of the magma, which will lead to crystal growth at the same time as bubbles form. We do not presume to include such effects, but simply recognise that they may be of significant importance.

The situation we consider is indicated in Fig. 1, which shows schematically a conduit flow from a magma chamber towards the surface. The chamber may have a foam layer at its roof, which feeds into a counter-current two-phase flow in the conduit, with an exsolving bubble-rich central flow rising through a bubble-poor downwelling flow. The cartoon shows also a transition from this counter-current bubbly flow to a *churn* flow, in which there are also large Taylor bubbles, and no clear separation between the up- and down-flows. We think of the exsolved gas as steam, although there will be other dissolved gases, in particular, CO_2. Additionally (and particularly as steam is exsolved), crystals will

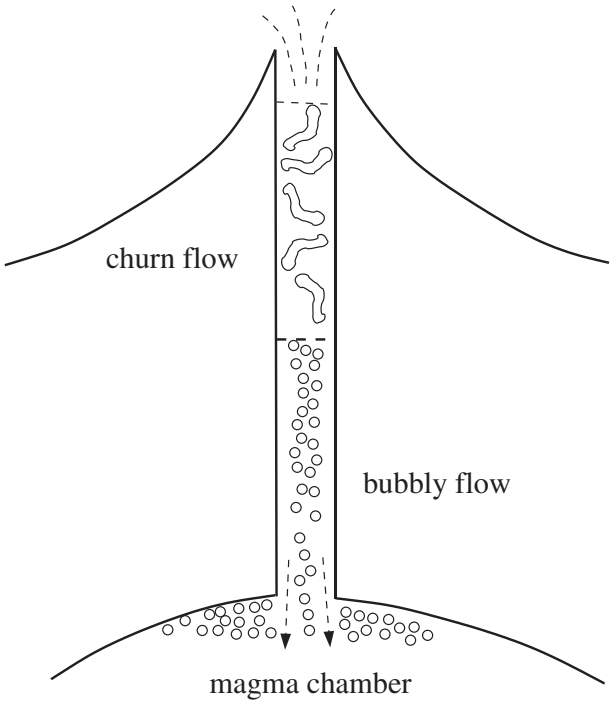

Fig. 1. A cartoon of the conduit flow from the magma chamber. We show a régime transition between bubbly counter-current flow and churn flow, which we later find to be necessary in a steady state description.

grow in the melt (Sparks, 2003). We ignore this also. Initially, for simplicity, we will consider a two-dimensional flow described by horizontal and vertical coordinates x and z, respectively. Extension to cylindrical pipe flow will be done later in Section 3.4.

In a two-phase flow model, the average gas and liquid pressures are generally different, and the difference is usually constituted in terms of the phase velocities (Drew and Passman, 1999). This includes terms representing bulk viscosity and bubble collapse (Batchelor, 1967, pp. 253, 480), as well as surface tension. In an earlier draft of this paper, many such terms were included, and then it was shown through scaling arguments that they were all small in comparison to the pressure difference along the conduit, so we will take the pressures to be equal.

The magma consists of two components, liquid magma and gaseous steam, having respective densities ρ_l and ρ_g. The gas volume fraction is α, and the mass fraction of dissolved water in the magma is c. As the magma ascends, exsolution occurs at a rate E (with units of kg steam per unit volume per unit time), and therefore mass conservation of the liquid and gas phases can be written in the form

$$\begin{aligned}&[\rho_l(1-\alpha)]_t + \nabla.[\rho_l(1-\alpha)\mathbf{u}] = -E,\\ &(\rho_g\alpha)_t + \nabla.(\rho_g\alpha\mathbf{v}) = E,\end{aligned} \tag{1}$$

The sum of these represents conservation of total mass, i.e., of the non-aqueous magma and the water substance component. Additionally we also have conservation of mass of total water substance, whose density is $\rho_l(1-\alpha)c + \rho_g\alpha$, or alternatively, conservation of non-aqueous magma, whose density is $\rho_l(1-\alpha)(1-c)$; selecting the latter, we have therefore

$$[\rho_l(1-\alpha)(1-c)]_t + \nabla.[\rho_l(1-\alpha)(1-c)\mathbf{u}] = 0, \tag{2}$$

where $\mathbf{u}$ is the liquid velocity, $\mathbf{v}$ is the gas velocity, and combining this with Eq. $(1)_1$ (we use the notation $(a)_b$ to represent the b-th member of the equation set (a)), we obtain

$$[\rho_l(1-\alpha)c]_t + \nabla.[\rho_l(1-\alpha)c\mathbf{u}] = -E. \tag{3}$$

There are two momentum equations, and these take the form

$$\begin{aligned}&[\rho_l(1-\alpha)\mathbf{u}]_t + \nabla.[\rho_l(1-\alpha)\mathbf{u}\mathbf{u}] = -(1-\alpha)\nabla p + \nabla.\left[\mu_l(1-\alpha)\left(\nabla\mathbf{u} + \nabla\mathbf{u}^T\right)\right] + \mathbf{M} - \rho_l(1-\alpha)g\mathbf{k},\\ &(\rho_g\alpha\mathbf{v})_t + \nabla.(\rho_g\alpha\mathbf{v}\mathbf{v}) = -\alpha\nabla p - \mathbf{M} - \rho_g\alpha g\mathbf{k},\end{aligned} \tag{4}$$

where p is the pressure, μ_l is the liquid viscosity, which we begin by taking to be independent of dissolved water content, $g \approx 9.8\,\mathrm{m\,s^{-2}}$ is acceleration due to gravity, and $\mathbf{k}$ is the unit vector in the vertical direction. The term $\mathbf{M}$ is an interfacial drag term which will generally be proportional to $\mathbf{v}-\mathbf{u}$. One particularly useful assumption is to take

$$\mathbf{M} = \frac{\mu_l\alpha(1-\alpha)(\mathbf{v}-\mathbf{u})}{k}, \tag{5}$$

which is the appropriate form if the resultant equation for the gas momentum (neglecting acceleration) is equivalent to Darcy's law (for the liquid flow relative to the dispersed bubbles), with k being the permeability.

The liquid density ρ_l will depend on volatile concentration c, temperature T and pressure p. The first two of these dependences are small, but the last is significant (Huppert and Woods, 2002). On the other hand, magma density will depend even more on crystal fraction, which we do not consider in our model. For reasons of simplicity, we take ρ_l to be constant. We assume an ideal gas such that

$$\rho_g = \frac{M_w p}{RT}, \tag{6}$$

where $M_w = 1.8 \times 10^{-2}$ kg mol^{-1} is the molecular weight of H_2O and $R = 8.3$ J mol^{-1} K^{-1} is the gas constant.

In the Earth's asthenosphere, pressures are sufficiently high that all gases are dissolved in the liquid melt (i.e., $\alpha = 0$), but as the magma ascends and the hydrostatic pressure decreases, the magma becomes supersaturated in volatiles and bubbles will start to nucleate; first CO_2 comes out of solution, and then H_2O. At a depth of 10 km, most CO_2 has already exsolved (Burton et al., 2007), but H_2O continues to be exsolved in a conduit flow, so that c will decrease from its initial value $c|_{\alpha=0} = c_0$. We assume that an equilibrium exists between the amount of H_2O dissolved in the melt and the surrounding pressure which satisfies the experimental relationship

$$c = Kp^{\nu}, \tag{7}$$

where K is a solubility constant. Eq. (7) is a form of Henry's law, which expresses the equilibrium at a gas-liquid interface between the processes of dissolution and evaporation; its form is based on experimental observations. The exponent $\nu = 0.5$ for rhyolite and is 0.7 for basalt (Parfitt and Wilson, 2008); for basalt the value of K is approximately $K = 1.1 \times 10^{-3}$ MPa$^{-\nu}$. The liquid density will vary slightly as the gas is exsolved, but if c is small, the variation is small and will be ignored.

It is commonly the case in considering conservation of energy of each phase to assume that the interfacial heat transfer is so large that the gas and liquid temperatures are the same. In this case, we only need to consider conservation of total energy, and this is given approximately by (see Fowler, 2011, p. 845, for example)

$$\alpha\rho_g c_{pg}\frac{dT}{dt_g} + (1-\alpha)\rho_l c_{pl}\frac{dT}{dt_l} + LE = \nabla.[(1-\alpha)k_l\nabla T]; \tag{8}$$

the four terms in this equation represent advection of heat by the gas, advection of heat by the liquid, loss of latent heat due to exsolution, and thermal conduction of heat; here k_l is the thermal conductivity of the magma (that for water vapour being much less), c_{pg} and c_{pl} are the gas and liquid specific heats at constant pressure, L is the latent heat, which we take to be constant, and

$$\frac{d}{dt_l} = \frac{\partial}{\partial t} + \mathbf{u}.\nabla, \quad \frac{d}{dt_g} = \frac{\partial}{\partial t} + \mathbf{v}.\nabla. \tag{9}$$

It can be shown that other adiabatic terms involving pressure are small, on the basis that the variation of pressure along the conduit is much smaller than the variation of sensible heat, $\Delta p \ll \rho_l c_{pl}\Delta T$. The Eqs. (1), (3), (4), (6), (7) and (8) give us eight equations for the eight unknowns $\mathbf{u}$, p, α, ρ, ρ_g, E, T and c. Generally, the evaporation rate E is determined from the energy Eq. (8). This is commonly the case in two-phase phase change problems, since at thermodynamic equilibrium, the temperature is prescribed as the liquidus temperature of the melt. In the present case, this is not quite true, since the thermodynamic equilibrium is given by Eq. (7), which is independent of temperature, and thus E can be thought of as being determined by Eq. (3).

2.1. Bubbly flow

We initially assume a bubbly flow, which we expect to be appropriate for sufficiently small α. A major simplification of the two-phase model stems from the assumption that the interactive drag between the phases would be large if there were any significant velocity difference between the phases, not only in the gas momentum equation, but also in that for the liquid. In a viscously dominated flow, the appropriate vertical velocity scale is $\rho_l g a^2/\mu_l$, where a is the conduit radius (or half-width if a channel), and thus if we assume the drag to be of the form (5), we find that $\mathbf{M}/\rho_l g \sim a^2/a_b^2$, where a_b is bubble radius (since we have the permeability $k \sim a_b^2$). Typical bubble sizes in erupted scoria are of the order of 100 μm (Rust and Cashman, 2011), and in this case the assumption of a homogeneous flow in which the gas and liquid velocities are equal is a reasonable assumption, since $a_b \ll a$. We thus begin by taking $\mathbf{v} = \mathbf{u}$. To obtain an appropriate momentum equation, we thus need to add the two momentum equations to eliminate $\mathbf{M}$. This rough argument is elaborated more explicitly below, following Eq. (13).

2.2. Dimensionless model

The geometry and boundary conditions of the counter-current flow in the conduit are shown in Fig. 2. The figure shows the right hand side of a counter-current flow, with the centre of the flow at the left, and the conduit wall at the right. The upwelling flow (to the left of the diagram) is bubble-rich and hot, the downwelling flow (to the right) is bubble-poor and relatively cool. As mentioned above, we consider first flow in a two-dimensional channel; the extension to pipe flow is made later in Section 3.4. We define horizontal and vertical coordinates x and z, with corresponding velocity components $\mathbf{v} = \mathbf{u} = (u, w)$, and the two-dimensional conduit occupies $-a < x < a$, $0 < z < l_c$. We make the model dimensionless in the following way. The notation $x \sim a$ below signifies that we define a dimensionless length variable x^* by means of the relation $x = ax^*$, and so on for the other variables; in the resulting dimensionless equations, the asterisks are then omitted for convenience;

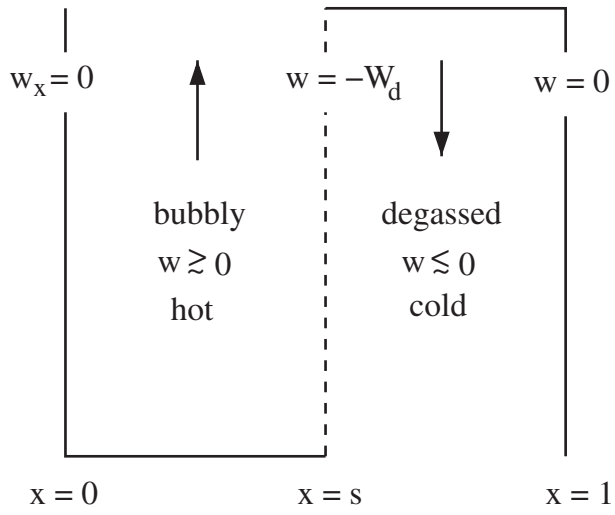

Fig. 2. The geometry and boundary conditions of the flow. The cartoon shows the dimensionless half-width of the channel, with the centre-line at $x = 0$, the interface between bubbly and degassed flow at $x = s$, and the conduit wall at $x = 1$.

the slight exception to this is in the definition of the dimensionless conduit length l^*, where the asterisk is retained to avoid confusion with the length scale l. The model is made dimensionless using the scalings

$$x \sim a, \quad z \sim l, \quad w \sim v_0 \equiv \frac{\rho_l g a^2}{\mu_l}, \quad u \sim \frac{\rho_l g a^3}{\mu_l l}, \quad \rho_g \sim \rho_g^0 = \frac{M_w \rho_l g l}{RT_c},$$
$$c \sim c_0, \quad T \sim T_c, \quad p = \rho_l g l \Pi, \quad E \sim \frac{\rho_g^0 \rho_l g a^2}{\mu_l l}, \quad t \sim \frac{\mu_l l}{\rho_l g a^2}, \quad l_c = l l^*, \tag{10}$$

where l is a suitable length scale for the conduit (chosen precisely below), and T_c is the chamber temperature. The vertical velocity scale is chosen to provide a balance between the driving buoyancy of the ascending bubbly magma and the viscous stress which resists it, although it should be pointed out that the value of this scale is a lot larger than inferred ascent rates of ~0.3 m s^{-1} (Burton et al., 2007), which they deduce from the magma flux necessary to produce observed SO_2 emissions.

The non-dimensional Eqs. (1), (3), (4), (6) and (7) take the form

$$\begin{aligned}
(\rho_g \alpha)_t + \nabla.(\rho_g \alpha \mathbf{u}) &= E, \\
-\alpha_t + \nabla.[(1-\alpha)\mathbf{u}] &= -\delta E, \\
[(1-\alpha)c]_t + \nabla.[(1-\alpha)c\mathbf{u}] &= -\Gamma E, \\
c &= \chi \Pi^\nu, \\
\rho_g &= \frac{\Pi}{T}, \\
\varepsilon^2 G\rho(u_t + \mathbf{u}.\nabla u) &= -\frac{\partial \Pi}{\partial x} + \varepsilon^2\left(\frac{\partial^2 u}{\partial x^2} + \varepsilon^2 \frac{\partial^2 u}{\partial z^2}\right), \\
G\rho(w_t + \mathbf{u}.\nabla w) &= -1 - \frac{\partial \Pi}{\partial z} + \alpha(1 - \delta\rho_g) + \frac{\partial^2 w}{\partial x^2} + \varepsilon^2 \frac{\partial^2 w}{\partial z^2}, \\
\rho &= (1-\alpha) + \delta\alpha\rho_g.
\end{aligned} \tag{11}$$

The parameters are defined by

$$\varepsilon = \frac{a}{l}, \quad G = \varepsilon Gr, \quad Gr = \frac{v_0^2}{ga} = \frac{\rho_l^2 g a^3}{\mu_l^2}, \quad \delta = \frac{\rho_g^0}{\rho_l}, \quad \Gamma = \frac{\delta}{c_0}, \quad \chi = \frac{K(\rho_l g l)^\nu}{c_0}; \tag{12}$$

Gr is the Grashof number for the flow, thus G is a reduced Grashof number in a high aspect ratio flow. We now choose to specify the length scale by choosing $\Gamma = 1$, thus

$$l = \frac{RT_c c_0}{M_w g}, \quad l^* = \frac{M_w g l_c}{RT_c c_0}. \tag{13}$$

In order to demonstrate explicitly the reason why the model can be taken to be homogeneous, as described in Section 2.1, we render the vertical component of the gas momentum Eq. $(4)_2$ dimensionless, using the scales in Eq. (10). Denoting the gas vertical velocity as w and the liquid vertical velocity as W, the result of this is, in dimensionless terms,

$$\delta G(Ew + \dot{w}) = -\alpha\Pi_z - \frac{a^2}{k}\alpha(1-\alpha)(w-W) - \delta\alpha\rho_g, \tag{14}$$

where $\dot{w} = w_t + \mathbf{v}.\nabla w$; assuming $\delta \ll 1$ and $G \lesssim 1$, we see that the interfacial drag term dominates, and thus the flow can be taken to be homogeneous, if $k \ll a^2$; and since (see Section 2.1) $k \lesssim a_b^2$, we see that, as stated, the assumption of homogeneous flow is valid provided the bubble size $a_b \ll a$, the tube radius (or channel half-width).

The dimensionless temperature T satisfies the energy equation

$$G[1-\alpha+\alpha\gamma\rho_g]\frac{dT}{dt} + \delta GSE = \frac{1}{Pr}\left[\{(1-\alpha)T_x\}_x + \varepsilon^2\{(1-\alpha)T_z\}_z\right], \tag{15}$$

where

$$Pr = \frac{\mu_l c_{pl}}{k_l}, \quad \gamma = \frac{\delta c_{pg}}{c_{pl}}, \quad S = \frac{L}{c_{pl}T_c}. \tag{16}$$

All of the model parameters are listed in Table 1, together with the values we use. Table 2 lists the dimensionless parameters and their approximate values. The neglect of $O(\varepsilon^2)$ terms yields the lubrication approximation $\Pi = \Pi(z,t)$. If we neglect other terms of order 10^{-2} and less except where they are singular, we obtain a reduced model, which is

$$\begin{aligned}
(\rho_g\alpha)_t + \nabla.(\rho_g\alpha\mathbf{u}) &= E,\\
-\alpha_t + \nabla.[(1-\alpha)\mathbf{u}] &= 0,\\
[(1-\alpha)c]_t + \nabla.[(1-\alpha)c\mathbf{u}] &= -\Gamma E,\\
c &= \chi\Pi^{\nu},\\
\rho_g &= \frac{\Pi}{T},\\
G(1-\alpha)(w_t + \mathbf{u}.\nabla w) &= -(1-\alpha) - \Pi_z + w_{xx},\\
G(1-\alpha)(T_t + \mathbf{u}.\nabla T) &= \frac{1}{Pr}\{(1-\alpha)T_x\}_x.
\end{aligned} \tag{17}$$

We have retained the small thermal diffusivity term to allow description of the thermal boundaries separating the upflow and downflow. Note that the Reynolds number of the flow in terms of the vertical velocity scale is just the (unreduced) Grashof number

$$Gr = \frac{\rho_l^2 g a^3}{\mu_l^2}, \tag{18}$$

Table 1
Parameters and their typical values. The values of T_a and T_c are taken from Harris and Stevenson (1997), and the viscosity values from Métrich et al. (2001); the low value is typical of crystal-free upwelling basaltic magma, and the higher value is more typical of downwelling crystal-rich gas-poor magma. The value of the surface tension σ (used later in Eq. (56)) is from Mangan and Sisson (2005).

Parameter	Meaning	Value used
a	Conduit radius	2 m
c_0	Initial mass fraction of dissolved water	0.05
c_{pl}	Liquid specific heat	10^3 J kg^{-1} K^{-1}
c_{pg}	Gas specific heat	2×10^3 J kg^{-1} K^{-1}
g	Gravity	9.8 m s^{-2}
k_l	Liquid thermal conductivity	1.8 W m^{-1} K^{-1}
K	Coefficient in Henry's law (7)	1.1×10^{-3} MPa$^{-\nu}$
L	Latent heat of exsolution	10^6 J kg^{-1}
l	Conduit length *scale*	3 km
M_w	Molecular weight of water	1.8×10^{-2} kg mol^{-1}
p_a	Atmospheric pressure	10^5 Pa
R	Universal gas constant	8.3 J K^{-1} mol^{-1}
T_c	Magma chamber temperature	1273 K
T_a	Surface magma temperature	1173 K
μ_l	(Range of) magma viscosity	20–1.4×10^4 Pa s
ν	Exponent in Henry's law (7)	0.7
ρ_g^0	Reference gas density	130 kg m^{-3}
ρ_l	Magma density	2.6×10^3 kg m^{-3}
ρ_s	Rock density	3.5×10^3 kg m^{-3}
σ	Gas-liquid surface tension	0.05 N m^{-1}

Table 2
Dimensionless parameters and values. The range of G is associated with the different viscosities of upwelling (high G) and downwelling (low G) flow. Equivalent ranges would apply to the value of Pr; the value quoted is for $\mu_l = 10^2$ Pa s, but Pr is in any case large.

Parameter	(Dimensionless) meaning	Value
G	Reduced Grashof number	0.17×10^{-2} – 0.9×10^{3}
Pr	Prandtl number	10^4
S	Stefan number	0.8
γ	Specific heat capacity ratio	0.03
Γ	Chooses conduit length scale	$\equiv 1$
δ	Density ratio	0.05
ε	Conduit aspect ratio	0.67×10^{-3}
η	Viscosity ratio	1.4×10^{-3}
λ	Relative temperature decrease	0.08
ν	Exponent in Henry's law	0.7
χ	Coefficient in Henry's law	0.46
Π_a	Surface pressure	1.3×10^{-3}

and since $\varepsilon \sim 10^{-3}$ and $G = \varepsilon Gr$, the flow is apparently laminar if $G \lesssim 1$. Small values of G are appropriate for degassed viscous magma, and we expect that this is the value which determines the mixing of the two magmas, because of the basic principle that in the motion of two fluids, the more viscous one controls proceedings because it is harder to move; for example, in the study of water waves, one generally ignores the air (unless it is driving the flow) on the basis that it is easily deformed. In addition, the different viscosities will cause the upwelling flow to be significantly narrower than the downwelling return flow, so that the upwelling flow Reynolds number will practically be similar to that of the downwelling flow. On this basis we assume that the flow is laminar, and we neglect mixing, although some will inevitably occur.[1]

Now if

$$\begin{aligned} \phi_t + \nabla.(\phi \mathbf{u}) &= 0, \\ \psi_t + \nabla.(\psi \mathbf{u}) &= 0, \end{aligned} \tag{19}$$

then it follows that

$$\left(\frac{\phi}{\psi}\right)_t + \mathbf{u}.\nabla\left(\frac{\phi}{\psi}\right) = 0. \tag{20}$$

Applying this to Eq. (17), we see that, bearing in mind that $\Gamma = 1$, $c + \frac{\rho_g \alpha}{1-\alpha}$ is advected with the flow. Indeed, we can suppose that this is also true within the magma chamber. Since, by choice of the scale for c, $c = 1$ when $\alpha = 0$ before exsolution occurs, it follows that the value of this conserved quantity is one (for the bubbly flow: zero for the degassed magma). We will suppose that at the base of the conduit, bubbles are either already present in the chamber, or just start to form at the entrance to the conduit: thus $\alpha|_{z=0} \geq 0$. The alternative, that bubble nucleation does not begin until further up the conduit, is unlikely, since only thermal buoyancy could then drive the flow, which would thus be more prone to stagnate and freeze.

From the definitions of c and ρ_g in Eq. (17), we can take (with $T = 1$, corresponding to an upflow temperature equal to that in the chamber)

$$\chi \Pi^{\nu} + \frac{\alpha \Pi}{1-\alpha} = 1, \tag{21}$$

and thus

$$\alpha = \frac{1 - \chi \Pi^{\nu}}{1 - \chi \Pi^{\nu} + \Pi}. \tag{22}$$

The function $\alpha(\Pi)$, which describes the variation of the bubble volume fraction with dimensionless pressure, is portrayed in Fig. 3. Assuming atmospheric pressure at the surface, a suitable boundary condition is to specify

$$\Pi = \Pi_a = \frac{p_a}{\rho_l g l} \quad \text{at} \quad z = l^*, \tag{23}$$

where l^* is the dimensionless conduit length, having been scaled with the length scale l defined in Eq. (13), $p_a = 10^5$ Pa is atmospheric pressure, which also implies $\alpha \approx 1$ there, since $\Pi_a \sim 10^{-3}$; all the gas exsolves at the surface. We come to this observation later.

[1] It turns out that the assumption $G \lesssim 1$ is actually quite safe, since the numerically computed values of $w \sim 10^{-3}$, so that the Reynolds number is indeed small, and this also resolves the discrepancy noted earlier between the choice of velocity scale and observed conduit velocities.

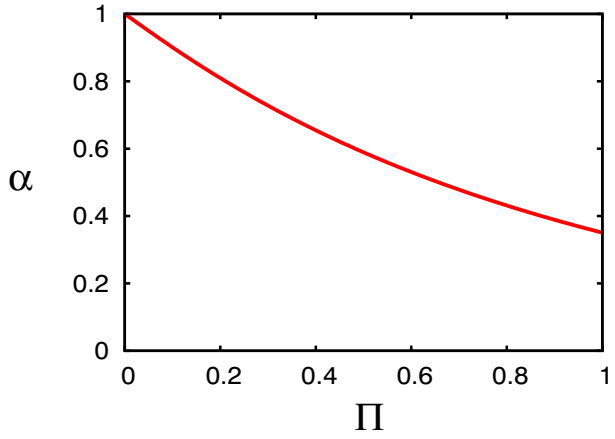

Fig. 3. The function $\alpha(\Pi)$ defined by Eq. (22), using the values $\chi = 0.46, \nu = 0.7$. α is the bubble volume fraction, Π is the dimensionless pressure, and χ and ν are dimensionless parameters defined in Eq. (12) and Table 1, respectively.

In addition, we need a boundary condition at the inlet. One possibility should be to prescribe the magma pressure in the chamber. This would imply

$$\Pi = \Pi_0 \quad \text{at} \quad z = 0, \tag{24}$$

where the simplest assumption would be that of a lithostatic pressure in the chamber,

$$\Pi_0 \approx \frac{\rho_s l^*}{\rho_l} \sim 1.35 l^*, \tag{25}$$

according to the values in Table 1, where ρ_s is the density of the crustal rock. An alternative is to prescribe the upwards mass flux at the inlet, since this is approximately known (Burton et al., 2007). More properly, the inlet boundary condition requires a consideration of the chamber filling process. We offer some comments on this in Section 4, although a complete discussion is beyond the scope of the present paper.

The application of Henry's law, and thus the validity of Eq. $(17)_4$, requires that $\alpha > 0$. Assuming no entrainment, this requires upflow, since when the bubbles reach the top of the conduit, they erupt or fizz into the atmosphere. In the descending flow, we presume that $\alpha = 0$, and Eq. $(17)_4$ does not apply.

In summary, our analysis shows that we can take the bubble volume fraction α to be an algebraic function of the pressure variable Π in the upwelling magma. This opens the path to solving the counter-current flow equations, which we treat in the next section.

3. Fully developed velocity profile

Initially, and for ease of exposition, we suppose that the viscosity takes the same value for both up and down flow; this restriction is relaxed later. We assume that the central portion of the conduit contains the ascending magma and we refer to this region as the upwelling zone. This is surrounded by the downwelling zone, where the degassed magma descends back to the chamber and we assume that there is no mixing at the upwelling-downwelling interface, which we denote (in $x > 0$) by $x = s$. We take the centre line to be at $x = 0$ and the bounding wall at $x = 1$. As we suppose the flow is symmetric about the centre line, this is sufficient for our needs. See Fig. 2 for an illustration of the geometry.

An interesting question concerns the velocity at the interface between the bubbly upwelling magma and the degassed downwelling magma. In their study, Kazahaya et al. (1994) assumed that the vertical velocity was zero at the interface. While this seems reasonable, it is not the most general assumption, and was thought by Stevenson and Blake (1998) to be the reason why their experimental results disagreed with the Kazahaya theory, a view endorsed by Huppert and Hallworth (2007). In our analysis, we allow for a non-zero interfacial velocity. The problem is somewhat similar to the counter-current flow in a settling pint of Guinness, where the inwards slope of the vessel wall causes the bubbles to sink with the fluid on the outside, although they rise in the interior (Benilov et al., 2013).

We now consider steady solutions of the reduced model of the preceding section. It is convenient to define a reduced temperature θ via

$$T = 1 - \lambda + \lambda\theta, \tag{26}$$

where

$$\lambda = \frac{\Delta T}{T_c}, \quad \Delta T = T_c - T_a, \tag{27}$$

and T_a is the magma temperature at the upper surface of the conduit; its value is determined by the heat losses from the surface and to the surrounding country rock. The point is that then $\theta = 1$ at the chamber, and $\theta = 0$ at the surface. In summary, the model describes a bubbly, mostly upwelling, flow (u, w) in $0 < x < s$, in which

$$\begin{aligned}
&[(1-\alpha)u]_x + [(1-\alpha)w]_z = 0,\\
&G(1-\alpha)(uw_x + ww_z) = -1 - \Pi' + \alpha + w_{xx},\\
&G(1-\alpha)(u\theta_x + w\theta_z) = \frac{1}{Pr}[(1-\alpha)\theta_x]_x,
\end{aligned} \tag{28}$$

with α given by Eq. (22). E no longer appears in the model as it has been used to determine c and thus α in Eq. (22) (see the discussion following Eq. (20)). In the (mostly) downwelling zone, $s < x < 1$, $\alpha = c = 0$, so that

$$\begin{aligned}
u_x + w_z &= 0,\\
G(uw_x + ww_z) &= -1 - \Pi' + w_{xx},\\
G(u\theta_x + w\theta_z) &= \frac{1}{Pr}\theta_{xx}.
\end{aligned} \tag{29}$$

Most studies of counter-current convection assume that the velocity field has reached a uniform state, in which viscous drag balances the buoyancy term, and we will follow this assumption. It is based on the notion that the inlet length $a\,Gr$ is much less than the conduit length, i.e., $G \ll 1$, and therefore the acceleration terms in Eqs. (28) and (29) are small. Considering Eq. (12), this condition is met most easily by taking the larger of the viscosity estimates in Table 1 (which we show to be the appropriate choice below). The flow is then uni-directional, $u = 0$, and w depends only on x. Such solutions have been provided before (e.g., Kazahaya et al., 1994; Huppert and Hallworth, 2007); the principal distinctions here are that the ascending fluid density varies as outgassing occurs, and thus also the radius or half-width of the ascending column of fluid varies with height.

The bubbly flow is contained in $0 \le x < s$ and the degassed flow in $s < x < 1$. The no slip condition at the conduit wall requires $w(1) = 0$, and the centre line symmetry requires $w_x(0) = 0$. In addition we require continuity of w and w_x at the interface. It follows from Eqs. $(28)_2$ and $(29)_2$ that

$$\begin{aligned}
w_{xx} &= 1 + \Pi' - \alpha, \quad x < s,\\
w_{xx} &= 1 + \Pi', \quad x > s.
\end{aligned} \tag{30}$$

Because the thermal diffusivity is so small, the ascending gas-rich magma is at the chamber temperature $\theta = 1$ and the descending degassed magma is at the surface temperature $\theta = 0$ (and also $\alpha = 0$). A thermal boundary layer separates the two regions, but its analysis distracts from, and is not necessary for, the analysis of the flow, and is relegated to the appendix.

We solve Eq. (30) subject to

$$w_x(0) = 0, \quad w(s) = -W_d, \quad w(1) = 0. \tag{31}$$

A simple integration then yields

$$w = \begin{cases} \frac{1}{2}(\alpha - 1 - \Pi')(s^2 - x^2) - W_d & \text{for } 0 \le x \le s,\\ -\frac{1}{2}(1 + \Pi')(s^2 - x^2) + \alpha s(s - x) - W_d & \text{for } s \le x \le 1, \end{cases} \tag{32}$$

and the condition of no slip at $x = 1$ gives

$$\Pi' = -1 + \frac{2\alpha s}{1+s} + \frac{2W_d}{1-s^2}. \tag{33}$$

Lastly, it remains to determine the interface position s and the interfacial velocity W_d. The conditions to determine these come from integration of the mass conservation Eq. $(28)_1$, using conditions of $u = 0$ at $x = 0$ and $x = 1$, and no flow through the interface at $x = s$, i.e., $u = ws'$ there. One consequence of this is the condition of no net mass flux, which is approximately (since $\delta \ll 1$) that of no net liquid flow:

$$\int_0^1 (1-\alpha)w\,dx = 0, \tag{34}$$

where the constant on the right hand side is zero because of equal up and down flow at the top and bottom. By integrating only from $x = s$ to $x = 1$, we find that the downwards degassed flux is independent of height, thus

$$Q_+ = -\int_s^1 w\,dx = Q^* \tag{35}$$

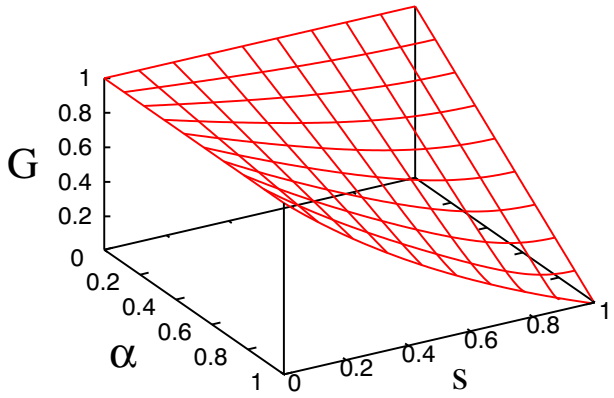

Fig. 4. The surface $G(\alpha, s)$. This function, of bubble volume fraction and upwelling flow half-width, is given by Eq. (38), and represents the negative of the dimensionless vertical pressure gradient Π' in the conduit, i.e., the pressure gradient scaled by the magmastatic value. Since $0 < G < 1$, $-1 < \Pi' < 0$. A value of zero indicates a constant pressure in the conduit, while a value of -1 indicates a magmastatic pressure.

(this defines Q_+), where Q^* is constant (and either to be determined or prescribed from the appropriate inlet condition). Using Eqs. (32) and (33), these conditions lead to the pair of relations

$$\begin{aligned} \alpha s(1-s)^2\left[(1-2\alpha)s^2+2s-1\right] &= 2W_d(\alpha s^3-3\alpha s+2), \\ \frac{\alpha s(1-s)^3}{6(1+s)}+\frac{W_d(2-s-s^2)}{3(1+s)} &= Q^*, \end{aligned} \tag{36}$$

and solving these yields

$$\begin{aligned} W_d &= \frac{\alpha s(1-s)^2\left[(1-2\alpha)s^2+2s-1\right]}{2\left(\alpha s^3-3\alpha s+2\right)}, \\ Q^* = Q_+(\alpha,s) &\equiv \frac{\alpha(1-\alpha)s^2(1-s)^3(3+s)}{6\left(\alpha s^3-3\alpha s+2\right)}. \end{aligned} \tag{37}$$

A distinction from earlier work (Huppert and Hallworth, 2007) is that the upwelling half-width s is not prescribed, but must be determined from Eq. $(37)_2$.

Finally, our plan, in principle, is this. Eq. $(37)_1$ allows us to write Eq. (33) in the form

$$\Pi' = -\left[1-\frac{\alpha s\left\{3(1-s)^2+2(1-\alpha)s(3-2s)\right\}}{2(1-\alpha)+\alpha(1-s)^2(2+s)}\right] = -G(\alpha,s), \tag{38}$$

and $-1 < \Pi' < 0$, see Fig. 4; Eq. (22) defines $\alpha(\Pi)$ as a monotonic function. For a given value of Q^*, Eq. $(37)_2$ defines $s(\alpha; Q^*)$. Thus we solve $\Pi' = -G[\alpha(\Pi), s\{\alpha(\Pi), Q^*\}] \equiv -g(\Pi; Q^*)$, and we solve this subject to the entry boundary condition $\Pi = \Pi_0$ at $z = 0$; then the value of Q^* is chosen in order to satisfy the exit condition $\Pi = \Pi_a$ at $z = l^*$. Alternatively, we prescribe Q^* at the inlet, and this determines the inlet pressure Π_0.

There are two evident difficulties with this strategy. The first lies in the inversion of Eq. (37). The function $Q_+(\alpha, s) > 0$ is concave in both α and s (essentially it behaves like $\alpha(1-\alpha)s^2(1-s^3)$), and so constant Q_+ contours (for $Q_+ \lesssim 0.004$)[2] take the form of closed loops in (α, s) space. An example is shown in Fig. 5, for $Q_+(\alpha, s) = 0.003$. Thus there are two possible choices for s, which we denote as $s_+(\alpha)$ and $s_-(\alpha)$, corresponding to the upper and lower branches of the contour

$$Q_+(\alpha, s) = Q^*. \tag{39}$$

The question is, which should we choose?

The second issue concerns the fact that for given Q^*, s is only defined for a finite range of α; thus not all values of Q^* allow α to reach $\alpha(\Pi_a) \sim 0.999$. This is discussed further in Section 3.2 below.

[2] It is because $Q_+ \sim 10^{-3}$ that $w \sim 10^{-3}$, as mentioned in an earlier footnote.

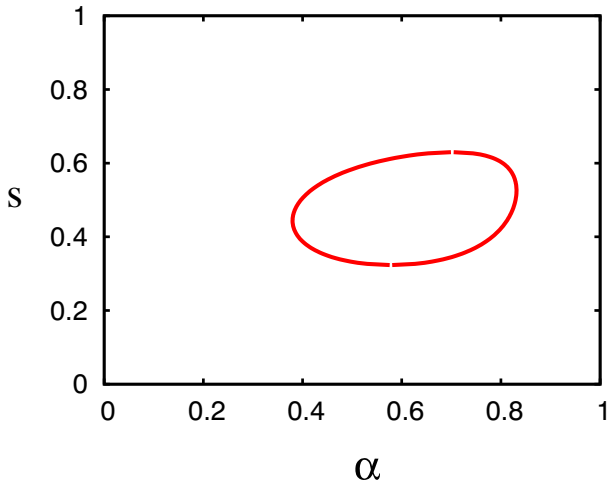

Fig. 5. The contour $Q_+(\alpha, s) = 0.003$. The value of Q_+ is the downwards flux of degassed magma (see Eq. (35)), and so for a prescribed value of this equal to 0.003, the contour indicates the dependence of the upwelling flow half-width s on the bubble volume fraction α.

3.1. Entrance relaxation

The fact that there are two possible values of s is a problem because it is not then clear which to choose; and if both are possible, which will occur in practice. A simple analogy can provide some insight here. A simple logistic population model for a population of size $u(t)$ is

$$\tau \dot{u} = u(K - u), \tag{40}$$

where τ is the natural growth time and K is the carrying capacity. If τ is small, we might neglect the derivative term, and then we have two possibilities: $u = 0$ and $u = K$. In this case, the correct solution ($u = K$) is selected because the derivative term shows that it is stable, while $u = 0$ is unstable.

Confronted by the multiplicity (an *isola*) indicated in Fig. 5, the most natural resolution is therefore that some rapid relaxation process has been neglected, and in the present case, the most obvious candidate is the neglect of the inertial relaxation terms proportional to G. We now give a suggestive argument that indicates that this is the case.

First note that in a laboratory experiment, one might devise an apparatus in which both α and s are prescribed at the inlet; this suggests that s should satisfy a differential equation (whose steady solution would thus be Eq. (39)). Our argument below suggests that this is the case.

Returning to Eqs. (28) and (29), we have exactly

$$\begin{aligned} 0 &= -(1 + \Pi' + M_u - \alpha)\, s + w_x|_s, \\ 0 &= -(1 + \Pi' + M_d)\,(1 - s) + [w_x]_s^1, \end{aligned} \tag{41}$$

where

$$\begin{aligned} M_u &= \frac{G(1-\alpha)}{s} \frac{d}{dz} \int_0^s w^2 \, dx, \\ M_d &= \frac{G}{(1-s)} \frac{d}{dz} \int_s^1 w^2 \, dx, \end{aligned} \tag{42}$$

and these are functions of z. We now make the assumption that, consistently with Eq. (42),

$$\begin{aligned} 0 &= -(1 + \Pi' + M_u - \alpha) + w_{xx}, \quad x < s, \\ 0 &= -(1 + \Pi' + M_d) + w_{xx}, \quad x > s, \end{aligned} \tag{43}$$

throughout the flow (this is a kind of Pohlhausen approximation). We can then integrate as before. Omitting algebraic details, we find that the conserved quantity

$$Q^* = \int_0^s (1 - \alpha) w \, dx \equiv (1 - \alpha) s \overline{w_u}, \tag{44}$$

or

$$Q^* = -\int_s^1 w\,dx \equiv -(1-s)\overline{w_d}, \tag{45}$$

satisfies

$$Q^* = -\frac{s^3(1-s)^2(2+s)\Delta M}{3(\alpha s^3 - 3\alpha s + 2)} + Q_+(\alpha, s), \tag{46}$$

where

$$\Delta M = M_u - M_d. \tag{47}$$

To calculate this, we make the assumptions (bearing in mind Eqs. (44) and (45))

$$\begin{aligned}\int_s^1 w^2\,dx &= (1-s)\overline{w_d^2} \approx (1-s)\overline{w_d}^2 = \frac{Q^{*2}}{(1-s)},\\ \int_0^s w^2\,dx &= s\overline{w_u^2} \approx s\overline{w_u}^2 = \frac{Q^{*2}}{(1-\alpha)^2 s},\end{aligned} \tag{48}$$

and then Eq. (42) leads to

$$\Delta M \approx -Q^{*2}G\left[\frac{1}{(1-\alpha)s^3} + \frac{1}{(1-s)^3}\right]s', \tag{49}$$

where we can ignore derivatives of α on the basis that α varies relatively slowly. It then follows from Eq. (46) that an appropriate modification of Eq. (39) is

$$\kappa s' + Q_+(\alpha, s) = Q^*, \tag{50}$$

where

$$\kappa = \frac{(2+s)Q^{*2}G}{3(\alpha s^3 - 3\alpha s + 2)}\left[\frac{(1-s)^2}{1-\alpha} + \frac{s^3}{1-s}\right], \tag{51}$$

and is small and positive. This suggests that s rapidly relaxes to the lower branch of the $Q_+ = Q^*$ contour, and in fact we use Eq. (50) together with Eq. (38) in solving the model numerically.

The adoption of Eq. (50) raises the awkward question of what an appropriate boundary condition for s might be, and where it should be applied. Luckily, if $\kappa \ll 1$, the choice of boundary condition is not significant, and we argue in the following section that it should be applied at $z = 0$.

3.2. Churn flow

If we use the parameters χ, Π_a and ν in Table 2, then we find that at the surface, where $\Pi = \Pi_a$, and using the definition of c in Eq. (17), the dimensionless water concentration in the magma is ~0.01, corresponding (via the scale c_0 in Eq. (10)) to 0.05 wt. %, and the consequent bubble fraction (via Eq. (22)) is about 0.9986. Of course this assumes the empirical Eq. (7) is accurate down to atmospheric pressure, which is not really the case (measured values are nearer 0.1 wt. %), but this does not significantly affect the outlet void fraction. Such a high void fraction would be representative of a foam, but observations do not support this idea; rather, it is generally assumed that a transition to a slug or churn flow occurs in the conduit, where bubble coalescence leads to the formation of large Taylor bubbles, comparable in dimension to the width of the conduit (James et al., 2013). Slug and churn flow are particular types of two-phase flow which are associated with changes in gas and/or liquid mass flux. In both régimes the continuous phase is a bubbly liquid with small bubbles, but there are also large 'Taylor' gas bubbles; the size of these is typically comparable to the conduit diameter, and the distinction is that in slug flow, the Taylor bubbles almost fill the conduit, while in churn flow they do not, and the flow consequently appears more disordered (hence the alternative description as 'churn-turbulent' flow). The transition from bubbly to slug or churn flow is typically associated with an increase of bubble volume fraction beyond some critical value (Montoya et al, 2016), with this transition being to slug flow in narrow conduits, but more likely to churn flow in wide conduits. Alternatively, volcanologists visualise the magma becoming 'permeable' at large gas fractions (Burton et al., 2007), although such terminology must be used carefully. The two concepts are not so different, insofar as they both involve the coalescence of bubbles; it is only the the geometric nature of the resulting structures which is at issue: whether they form discrete Taylor bubbles, or filamentary stringers which combine to form a connected pathway.

Typical vesicularities in erupted scoria from a range of different eruptions and magma types are of the order of 80% (i.e., $\alpha = 0.8$) (Rust and Cashman, 2011), and we might initially suppose that this represents the small bubble fraction in the liquid magma in a churn or slug flow.

On the other hand, it is more likely that a transition to churn flow occurs at a much lower value (0.3–0.5) (Burton et al., 2007; Ishii and Zuber, 1979), so that the observed vesicularities include both the small bubble fraction and a portion of the filamentary structures, as seen by Burton et al. (2007, Fig. 5).

We will suppose that transition to churn or filamentary flow occurs at a critical value α_c of the small bubble fraction, and this suggests that this is also where the counter-current flow becomes a churn flow; evidently this occurs for $z < l^*$, and it is then necessary to model the churn flow in the upper part of the conduit.

We now turn to a two-phase flow model which can represent churn or slug flow. We reconsider Eqs. (1), (3) and (4), but now we suppose that the flow consists of bubbly liquid together with Taylor bubbles of radius a_b which are sufficiently large (comparable to the conduit diameter) that the discussion in Section 2.1 suggests that phase separation is significant, thus $\mathbf{v} \neq \mathbf{u}$. On the other hand, the flow is now thoroughly mixed, and a cross-sectionally averaged model is appropriate; in particular, the effect of viscous resistance of the liquid is modelled by a wall friction term, the variables are cross-sectionally averaged so that the average horizontal velocity is zero, and there are no horizontal derivatives. We thus modify Eqs. (1), (3) and (4) to the form

$$\begin{aligned}
[\rho_l(1-\beta)(1-\alpha)]_t + \frac{\partial}{\partial z}[\rho_l(1-\beta)(1-\alpha)w] &= -E,\\
(\rho_g(1-\beta)\alpha)_t + \frac{\partial}{\partial z}(\rho_g(1-\beta)\alpha w) &= E-A,\\
(\rho_g\beta)_t + \frac{\partial}{\partial z}(\rho_g\beta v) &= A,\\
[\rho_l(1-\beta)(1-\alpha)c]_t + \frac{\partial}{\partial z}[\rho_l(1-\beta)(1-\alpha)cw] &= -E,\\
\rho_l(1-\beta)(1-\alpha)(w_t+ww_z)+\rho_g[(1-\beta)\alpha+\beta](v_t+vv_z)+A(v-w) &= -p'-\frac{\tau_w}{a}-[\rho_l(1-\beta)(1-\alpha)+\rho_g\{(1-\beta)\alpha+\beta\}]g,\\
M &\approx -\beta p'-\rho_g\beta g,
\end{aligned} \tag{52}$$

where β is the large bubble fraction, A is a bubble aggregation rate, the bubbly liquid momentum equation has been simplified by using the first three mass conservation equations, τ_w is the wall stress, divided here by conduit radius a, which is the appropriate hydraulic radius for the flow, and we neglect the acceleration terms in the gas momentum equation. Here v is the vertical large bubble velocity and w is the vertical bubbly liquid velocity.

The choice of a Darcy-like expression for M as in Eq. (5) is no longer appropriate, as the drag is likely to be inertia-dominated. A suitable expression is given by Montoya et al (2016), and is

$$M = \frac{\frac{3}{4}\beta\rho_l c_D|v-w|(v-w)}{d_b}, \tag{53}$$

where $d_b = 2a_b$ is bubble diameter, and c_D is a drag coefficient. This expression is equivalent to Ergun's equation (Ergun and Orning, 1949) describing rapid flow past packed spheres, and Ergun and Orning suggest

$$c_D = \frac{\beta B}{(1-\beta)}, \tag{54}$$

with values of $B \sim 1$ – 5.[3] However, the configuration of the flow in a packed bed is quite different to that of a churn flow. Indeed, for a percolative filamentary flow, the gas forms the continuous phase, which might suggest $c_D \to 0$ as $\beta \to 1$.

This last assumption is mirrored by other parameterisations of c_D. Ishii and Zuber (1979), for example, suggest

$$c_D = \frac{8}{3}\beta(1-\beta)^2 \tag{55}$$

(translating their Eq. (21)). Chen et al. (2009, Eq. (4)) suggest $c_D \propto (1-\beta)^4$. Such expressions may be little more than suggestive for the case of a vesiculating magma, where the apparent onset of percolation at gas fractions ~0.8 suggests a rapid reduction in c_D at that value. We take this into consideration below.

Montoya et al.'s more general description suggests that c_D is a complicated function of the dimensionless parameters

$$Re = \frac{\rho_l d_b|v-w|}{\mu_l}, \quad E\ddot{o} = \frac{g\Delta\rho\, d_b^2}{\sigma}, \quad Mo = \frac{g\mu_l^4\Delta\rho}{\rho_l^2\sigma^3}, \tag{56}$$

[3] This follows from Eq. (6) of Ergun and Orning, noting that the specific surface area for spheres is $S_v = 6/d_b$, that u in their formula is the superficial velocity, and where for isolated Taylor bubbles, we identify the continuous phase volume fraction as $\varepsilon = 1-\beta$. The range of B (their β) is in their Table 1.

these being the Reynolds, Eötvös and Morton numbers. Chen et al. (2009) give a complicated expression for c_D in terms of these, but the values in the present case are so extreme that these empirical correlations are unlikely to have much validity. Specifically, if we take the velocity scale to be that in Eq. (10), then $Re = Gr \sim 5$ for a viscosity of $\mu_l \sim 10^4$ Pa s, while the Eötvös number is $\sim 2 \times 10^6$, and then $Mo = \frac{Eö^3}{Gr^2} \sim 10^{18}$, well outside the range of Montoya et al.'s Fig. 3. In the absence of any clear indication, we will take c_D as an $O(1)$ number, but its reduction as β increases is important.

The Eq. (52) can be written in dimensionless form, scaled as in Eq. (10), which gives, in the steady state,

$$\begin{aligned}
(\rho_g \beta v)' &= A,\\
\{(1-\beta)(1-\alpha)w\}' &= -\delta E,\\
\{\rho_g(1-\beta)\alpha w\}' &= E - A,\\
\{(1-\beta)(1-\alpha)wc\}' &= -E,\\
G[(1-\beta)(1-\alpha) + \delta\{(1-\beta)\alpha + \beta\}]ww' + f\,Gr\,w^2 + \delta GA(v-w) &= -\Pi' - (1-\beta)(1-\alpha),\\
\frac{3c_D a\,Gr\,|v-w|(v-w)}{4d_b} &= -\Pi' - \delta\rho_g,
\end{aligned} \tag{57}$$

where we have taken

$$\tau_w = f\rho_l w^2. \tag{58}$$

Ignoring terms of order δ, G and $f\,Gr$ (typical values of the friction factor are $f \sim 0.005$), this leads to the approximate set (cf. Eq. (17))

$$\begin{aligned}
(\rho_g \beta v)' &= A,\\
(1-\beta)(1-\alpha)w &= -W,\\
(\rho_g(1-\beta)\alpha w)' &= E - A,\\
Wc' &= E,\\
-\Pi' &= (1-\beta)(1-\alpha),\\
\frac{3c_D a\,Gr\,|v-w|(v-w)}{4d_b} &= -\Pi',
\end{aligned} \tag{59}$$

where W is constant. The dimensionless temperature is taken to be constant in the churn flow, and equal to its surface value, thus $\theta = 0$, whence Eqs. $(17)_5$ and (26) imply

$$\rho_g = \frac{\Pi}{1-\lambda}. \tag{60}$$

In addition, we have Henry's law from Eq. $(17)_4$:

$$c = \chi\Pi^{\nu}. \tag{61}$$

At the transition interface (from bubbly to churn),

$$s = s_c, \quad \alpha = \alpha_c, \quad \Pi = \Pi_c \quad \text{at} \quad z = z_c. \tag{62}$$

The second, fifth and sixth equations in Eq. (59) can be written in the form

$$\begin{aligned}
(1-\beta)(1-\alpha)w &= -W,\\
v - w &= \Lambda,\\
-\Pi' &= (1-\beta)(1-\alpha),
\end{aligned} \tag{63}$$

where the new parameter is defined by

$$\Lambda = \left[\frac{4d_b(1-\beta)(1-\alpha)}{3c_D a\,Gr}\right]^{1/2}, \tag{64}$$

and is in general a function of β.

We assume that $\alpha = \alpha_c$ is constant (≈ 0.5), which thus serves to determine the aggregation rate. In Eq. (63), β is a function of Π, determined through the conservation law obtained by combining Eqs. $(59)_1$, $(59)_3$ and $(59)_4$ to eliminate E and A, together with Eqs. (60) and $(17)_4$. This leads to the implicit definition of β through

$$\beta\Lambda - \frac{\{(1-\beta)\alpha + \beta\}W}{(1-\beta)(1-\alpha)} = \frac{K + W\Pi^{\nu}}{\Omega\Pi}, \tag{65}$$

where K is a constant, and

$$\Omega = \frac{1}{\chi(1-\lambda)}. \tag{66}$$

To determine K and W, we use the fact that W is the net liquid downflow, and this is approximately zero (actually $O(\delta)$). However, the net volume flux of gas from the counter-current flow is $\alpha_c Q^*/(1-\alpha_c)$, and this is approximately equal to the left hand side of Eq. (65) at $z = z_c$, with a correction factor $(1-\lambda)$ to account for the small change in density across the transition due to the temperature jump (mass flux is conserved, not volume flux); thus we take

$$W = 0, \quad K = \frac{\Pi_c \alpha_c Q^*}{\chi(1-\alpha_c)}. \tag{67}$$

It follows that

$$\beta\Lambda = \frac{V_c}{\Pi}, \quad V_c = \frac{\alpha_c Q^* \Pi_c (1-\lambda)}{(1-\alpha_c)}. \tag{68}$$

We now consider the variation of the drag coefficient c_D with β. We follow the suggestion of Ishii and Zuber (1979) in Eq. (55) that c_D decreases as β approaches one. However we modify their expression to take account of the presumed dramatic reduction in drag when the vesicularity $\alpha + (1-\alpha)\beta$ reaches a critical value $\alpha^* \approx 0.8$ (Rust and Cashman, 2011), i.e., (presuming $\alpha = \alpha_c$)

$$\beta = \beta^* = \frac{\alpha^* - \alpha_c}{1-\alpha_c}. \tag{69}$$

To be specific, we suppose

$$c_D = c_D^0 (1-\beta)(\beta^* - \beta)^2 \tag{70}$$

(the inclusion of the cosmetic term $1-\beta$ is purely for convenience). More realistically, c_D will not approach zero as there is always some drag, but the effect is small and can be ignored. Then we have

$$\Lambda = \frac{\Lambda_0}{\beta^* - \beta}, \tag{71}$$

where

$$\Lambda_0 = \left[\frac{4 d_b (1-\alpha_c)}{3 c_D^0 a\, Gr}\right]^{1/2}, \tag{72}$$

and thus β is given by

$$\beta = \frac{\beta^* V_c}{V_c + \Lambda_0 \Pi}. \tag{73}$$

The function $\beta(\Pi)$ is illustrated in Fig. 6. It represents the variation of the large bubble volume fraction with the dimensionless pressure. As Π decreases, β increases as we would expect.

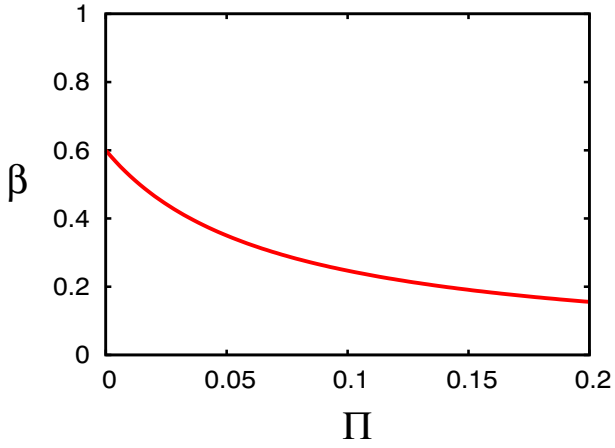

Fig. 6. The function $\beta(\Pi)$ defined by Eq. (73), using the values $\beta^* = 0.6$, $V_c = 0.007$, $\Lambda_0 = 0.1$; these are dimensionless parameters defined in Eqs. (69), (68) and (72): β is the large bubble volume fraction in churn flow, and Π is the dimensionless pressure.

3.3. Model summary

We now summarise our revised strategy to solve the model. If we are given an inlet pressure Π_0 at the chamber, we can then determine α_0 via Eq. (22). Select a value Q^* sufficiently small that there is a point (α_0, s_0) on the contour $Q_+(\alpha, s) = Q^*$ in Fig. 5. Given a value of the transition void fraction α_c, the $Q_+(\alpha, s) = Q^*$ contour also determines the critical values s_c and Π_c at the transition to churn flow at $z = z_c$, which is also to be found.

Next we integrate Eqs. (38) and (50) using the inlet boundary conditions (with $s = s_0$ there) until $\Pi = \Pi_c$, and this determines z_c. Following this, we integrate Eq. $(63)_3$ in $z > z_c$, with $\beta(\Pi)$ defined by Eq. (73), with $\Pi = \Pi_c$ at $z = z_c$, until $\Pi = \Pi_a$ at $z = l^*$. This then determines the actual length of the conduit in terms of the unknown Q^*. Given l^*, this serves to determine Q^*. In practice, it is convenient to think of Q^* as a parameter which is used to find the solutions for different conduit lengths, i.e., we assume Q^* and determine the consequent l^*. Of course, if instead we prescribe Q^*, then the inlet pressure has to be determined. We postpone providing numerical results for the model until we deal with the more realistic case of a cylindrical vent, and differing viscosities for the gas-rich and gas-poor magma.

3.4. Different viscosities and cylindrical conduits

Now we consider a cylindrical conduit, and we allow for the rising wet bubbly magma to have a lower viscosity μ_w than that of the downwelling dry magma, μ_d, based on the fact that the viscosity of a liquid magma is a strong function of its gas content. However, it should be noted that the viscosity of a foam can increase markedly over its parent liquid's viscosity as the bubble fraction increases (Wu et al., 1984; Princen and Kiss, 1989), and it is in fact possible that no major increase occurs, at least at large volume fraction. The parameter a is now the conduit radius, and we define the viscosity ratio

$$\eta = \frac{\mu_w}{\mu_d}. \tag{74}$$

For the range of values given for μ_l in Table 1 (i.e., from μ_w to μ_d), we have $\eta \sim 1.4 \times 10^{-3}$, but as mentioned above, η could be larger than this. The consequent modification of Eq. (30) can be written (where we choose to use μ_d as the viscosity in the scale choices in Eq. (10))

$$\begin{aligned} \eta\left(w_{rr} + \frac{1}{r}w_r\right) &= 1 + \Pi' - \alpha, \quad r < s, \\ \left(w_{rr} + \frac{1}{r}w_r\right) &= 1 + \Pi', \quad r > s, \end{aligned} \tag{75}$$

and the solution proceeds as before. We find successively

$$w = \begin{cases} \frac{\frac{1}{4}(1+\Pi'-\alpha)(r^2-s^2)}{\eta} - W_d, & r < s, \\ \\ \frac{1}{4}(1+\Pi')(r^2-s^2) - \frac{1}{2}\alpha s^2 \ln\left(\frac{r}{s}\right) - W_d, & r > s, \end{cases} \tag{76}$$

and equating the velocity to zero on the wall gives

$$W_d = \frac{1}{4}(1+\Pi')(1-s^2) + \frac{1}{2}\alpha s^2 \ln s. \tag{77}$$

Next we calculate the liquid upflow and downflow. The downflow is

$$Q_+ = -2\pi \int_s^1 rw\, dr = \frac{1}{8}\pi\left[(1+\Pi')(1-s^2)^2 - 2\alpha s^2(1-s^2+2s^2\ln s)\right], \tag{78}$$

and the upflow is

$$\begin{aligned} Q_- &= 2\pi(1-\alpha)\int_0^s rw\, dr \\ &= \frac{1}{8}\pi(1-\alpha)\left[\frac{\{\alpha-(1+\Pi')\}}{\eta}s^4 - 2s^2\{(1+\Pi')(1-s^2) + 2\alpha s^2\ln s\}\right]. \end{aligned} \tag{79}$$

Equating these, we find

$$1 + \Pi' = \frac{\alpha s^2\left[(1-\alpha)s^2 + 2\eta(1-s^2+2\alpha s^2\ln s)\right]}{(1-\alpha)s^4 + \eta(1-s^2)\{1+(1-2\alpha)s^2\}}, \tag{80}$$

and thus, with Eq. (79), we have

$$Q_+ = \frac{\frac{1}{8}\pi\alpha(1-\alpha)s^4\left[(1-s^2)(1-3s^2) - 4s^2\ln s - 4\eta(1-s^2)\{1-s^2+(1+s^2)\ln s\}\right]}{(1-\alpha)s^4 + \eta(1-s^2)\{1+(1-2\alpha)s^2\}}. \tag{81}$$

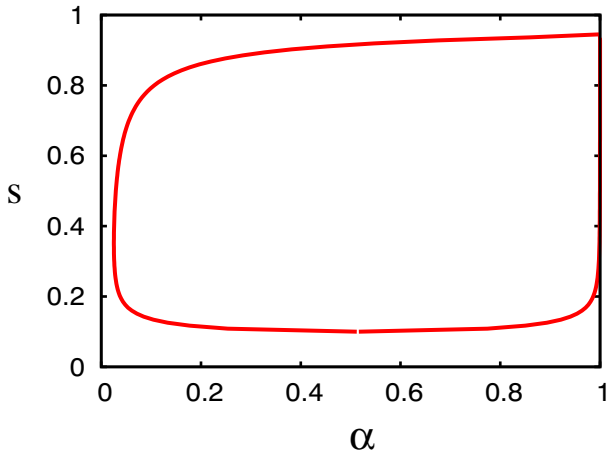

Fig. 7. The upwelling flow radius s versus the bubble volume fraction α, as given by Eq. (81), with the degassed liquid downflow $Q_+ = 0.01$ and the viscosity ratio of wet to dry magma $\eta = 0.001$.

As in the Cartesian case, the contours $Q_+ = Q^*$ form closed loops in α, s space. An example is shown in Fig. 7, which gives the variation of upwelling flow radius s as a function of bubble volume fraction α for a particular value of the downwelling dry magma flux. If we mimic the inlet relaxation as in Eq. (50), thus we specify

$$\kappa s' = Q^* - Q_+(s,\alpha), \tag{82}$$

then as before, s will follow the lower of the two equilibria (providing the initial value of s is sufficiently low). Values of Q^* can be inferred from measured values of gas flux M_g, for which we take a value of 37 kg s^{-1} (Burton et al., 2007). From Eq. (79), this corresponds to a dimensionless volume flux $\alpha Q_-/(1-\alpha)$, and in dimensional terms, using Eqs. (60) and (12) (with $\Gamma = 1$), we have

$$M_g = \rho_l c_0 v_0 a^2 \frac{\alpha Q^* \Pi_c}{(1-\alpha)}, \tag{83}$$

where we take $Q_- = Q^*$. Using the parameter values in the tables, and also $\mu_l = 10^4$ Pa s, $\alpha_c = 0.5$, we find $Q^* \approx 0.01$.

3.4.1. Churn flow

As before, we assume that there is a critical value α_c associated with a transition to churn flow. Because the churn flow model is cross-sectionally averaged, it is the same as in Eq. (59), and Π and β are determined as before by

$$\begin{aligned} \Pi' &= -(1-\alpha)(1-\beta), \\ \beta &= \frac{\beta^* V_c}{V_c + \Lambda_0 \Pi}. \end{aligned} \tag{84}$$

In summary, we solve the pair Eqs. (80) and (82) with $s = 0.5$ (for example; the precise value is not important for the solution) and $\Pi = \Pi_0$ at $z = 0$, given Q^*. The value of Q^* determines Π_c at the régime boundary, which thus also gives its location z_c. In $z > z_c$, we then solve Eq. $(84)_1$, taking $\alpha \equiv \alpha_c$ and Eq. $(84)_2$, until $z = \hat{l}$ where $\Pi = \Pi_a$. From this we define

$$\hat{\Pi} = \frac{\rho_s \hat{l}}{\rho_l} \tag{85}$$

(cf. Eq. (25)), and the object is to choose Q^* such that $\hat{\Pi} = \Pi_0$. Alternatively, we prescribe Q^*, and Π_0 is then determined.

A numerical solution quickly shows that the prospect of imposing an inlet pressure $\Pi_0 > 1$ is not possible. Indeed, it is clear from Eqs. (80) and (84) that $\Pi' > -1$, which implies that (since $\Pi_a \approx 0$) $\Pi_0 < \hat{l}$. The message is unfortunately obscured by its submergence in a sea of equations; but the message is simply stated. When the conduit is open, the frictional resistances to motion are negligible, and the only resistance of note is the weight of the magma itself. *This means that the inlet magma pressure is far below lithostatic, and is also less than (liquid) magmastatic.* One might wonder whether this result, that the magma pressure at the inlet to the conduit is less than magmastatic, might depend critically on certain assumptions in the model. For example, we assumed a transition to churn flow when the void fraction $\alpha = \alpha_c = 0.5$; but this assumption is not well constrained. However, other choices will have no effect on the conclusion, since the pressure gradient is below magmastatic in both counter-current and churn régimes, as can be seen from Eq. (38) (since $G < 1$) and Eq. (63).

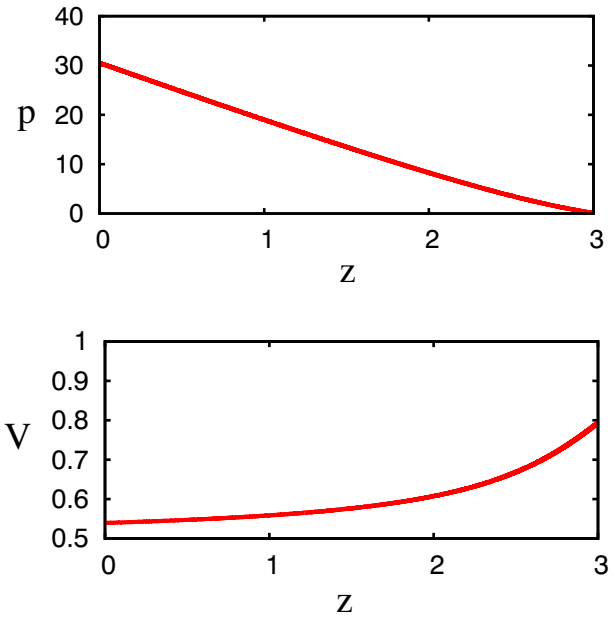

Fig. 8. Solutions for the dimensional pressure $p = \rho_l g l \Pi$ and the vesicularity (the total gas volume fraction) $V = \alpha + \beta - \alpha\beta$ as functions of dimensional height z for a cylindrical conduit, and with a viscosity ratio (wet to dry) of $\eta = 10^{-3}$, using values of the conduit length $l_c = 3$ km and the dimensionless dry magma downflux $Q^* = 10^{-2}$. Units: z in km, p in MPa, V dimensionless. Note that the scale for V is from 0.5 to 1.

Fig. 8 shows the profiles for a cylindrical conduit of $p = \rho_l g l \Pi$ and the vesicularity V (i.e., the total volume fraction of gas), defined by

$$V = \alpha + \beta - \alpha\beta, \tag{86}$$

for the particular choice $\eta = 10^{-3}$ and a conduit length of $l_c = 3$ km, and for a value of $Q^* = 10^{-2}$, which corresponds to observed mass flow rates (Burton et al., 2007).

For this choice of chamber depth, $\Pi_0 \approx 0.4 < \Pi_c = 0.657$, and there is no region of counter-current flow at all. The magma pressure reaches a value of 30 MPa at the inlet, compared to a magmastatic value of 76 MPa and a lithostatic pressure of 103 MPa. The magma chamber is thus severely underpressured.

It can be seen that the profile for p is approximately linear. This is due to Eq. (84), since $\alpha = \alpha_c$ is constant, and as indicated in Fig. 6, β varies slowly for $\Pi \gtrsim 0.1$, and the gradient only deviates from linear near the surface. If we select a longer conduit, so that there is a counter-current flow region, then the pressure gradient in the counter-current flow is also close to linear, $\Pi' \approx -(1 - \alpha)$, assuming that η is small, since α varies little, unless the conduit is very long.

4. Discussion

4.1. Counter-current two-phase flow

We began with the aim of placing the idea of counter-current flows in Strombolian conduits into a consistent model framework of two-phase flows. However, our investigation has led in increasingly orthogonal directions. Previous models have not included the dynamic effect of exsolution as the magma rises, and while two-phase models of magma rise have been presented in other contexts (Molina et al., 2012; Melnik, 2000), the present work is novel in this respect.

In our analysis of the bi-viscous counter-current flow, we use viscosity values (with ratio $\sim 10^3$) suggested by Métrich et al. (2001). A more recent analysis by Beckett et al. (2014) using detailed thermodynamic relationships suggests this ratio increases with depth, passing 10^2 at a conduit depth of some 3 km. On this basis, they suggest that the flow is only likely to be core-annular (as we have initially assumed) for depths greater than 3 km, but that shallower conduits may have side by side flow. This inference is based on experimental studies of counter-current flow (Beckett et al. 2011; Palma et al., 2011); however, it is noteworthy that these experimental results involve two liquids, and the wealth of flow régimes which are displayed by two-phase gas-liquid flows (Hewitt and Roberts, 1969; Wallis, 1969; Hetsroni, 1982) is not considered.

Our model makes the simplest initial assumption concerning two-phase flow, that is, that the flow is bubbly. We find that there are two possible states for the flow, and steady counter-current bubbly flow is not possible at very low or very high gas volume fraction. We provide a stability argument based on the inlet relaxation length which suggests that the flow with the narrower bubbly column is the stable one of these.

4.2. Churn flow

In practice, the non-existence of such flow at high or low void fraction α is not important, because it is likely that a bubbly foam is already created at the roof of the magma chamber. The non-existence at high void fraction suggests a breakdown of the bubbly flow régime to a churn-turbulent or slug flow, but such a transition is already known to occur at more moderate values of α. In fact, régime diagrams for (air/water) two-phase flow (Hewitt and Roberts, 1969)

suggest that for volume fractions larger than about 0.3, bubbly flow is unstable, and the flow undergoes transition (in narrow pipes) to slug flow (and later, churn and annular flow). Similar to flow in boiling tubes (e.g., Hetsroni, 1982), we surmise that the flow undergoes a similar régime transition as it rises through the conduit, although the critical value of $\alpha = \alpha_c$ where this occurs presumably depends on the properties of the magma, and its ability or inability to form a foam. For low viscosity basaltic magma in wide conduits, we expect a transition to churn-turbulent flow (Montoya et al, 2016).

The modelling of churn-turbulent flow in averaged two-phase flow models can be constructed in a similar way to models of bubbly flow, except that we now conceive of the vesicularity as consisting of small bubbles and larger Taylor bubbles, which may take the form of elongated filaments (Burton et al., 2007), which themselves may undergo a transition at elevated vesicularity to a connected and thus permeable régime. A conclusion concerning such flows is that they are quite simply represented, with the pressure drop being essentially magmastatic (using the reduced density associated with the vesicularity; indeed, this is also true for the bubbly flow), and observed erupted vesicularities can be fairly simply explained.

4.3. Magma under-pressure

However, an implication of the magmastatic pressure is that the magma chamber is severely underpressured. This point needs to be emphasised. Generally one would suppose that the magma pressure in the chamber would be close to the lithostatic pressure: otherwise the chamber ought to collapse. In a closed conduit where plugging and blow-out can occur, this seems fine; but in an open system, our results are strongly suggestive of a chamber pressure which is well below lithostatic. In our illustration of flow from a 3 km deep magma chamber, the chamber pressure is 30 MPa compared to a lithostatic pressure of 103 MPa. According to Burton et al.'s (2007) cartoon, the flow would already have become permeable at that stage. In contrast, our model suggests that, due to the reduction in drag coefficient as the percolation threshold is approached, this only happens at the surface.

The suggestion of low chamber pressures raises the issue of the dynamics of the magma chamber itself. In reality, the chamber and the conduit form a combined system, whose dynamics should properly be coupled to the flow in the conduit and the supply from underneath. Normally, the dynamics of the chamber is associated with the issue of eruptive periodicity, for which in explosive eruptions, the simple explanation is that magma supply from below causes overpressuring of the chamber until dike formation and eruption can occur (Blake, 1981; Tait et al., 1989).

4.4. Consequences for the magma chamber

In the present case, where we conceive of a permanently degassing chamber, it is less obvious what happens. The inferred liquid upflow of 570 kg s^{-1} in the conduit delivering its gas load of 37 kg s^{-1} would require a similar inflow to the chamber in order to exist in a steady state, but this would require chamber inflation, which would thus raise the chamber pressure, and the conduit flow could not be maintained. Alternatively, if the liquid inflow is such as to maintain mass balance, then the magma will become progressively depleted in volatiles.

A possible way of accommodating such depletion is to include the effect of crystallisation in the chamber, which has the effect of concentrating volatiles in the melt. Indeed, we might consider a chamber at late stage, full of crystals and acting more like a coherent crystal mush (Cashman and Giordano, 2014). Actually, portraits of the plumbing system of this type have been suggested by Métrich et al. (2010, Fig. 10) and more specifically by Suckale et al. (2016). Such a system also allows for the external lithostatic pressure to be supported by the crystals, while the potentially lower pore pressure allows for the possibility of compaction (McKenzie, 2011). The rate of viscous compaction (i.e., the rate of change of porosity) is $\propto \Delta p/\mu_s$ (Fowler, 1985), where Δp is the pressure difference between solid and liquid, and μ_s is the solid viscosity. With $\Delta p \sim 10^2$ MPa and $\mu_s \sim 10^{18}$ Pa s, this gives a time scale of 300 y for compaction to occur, though longer if the viscosity is higher: 30,000 y if $\mu_s \sim 10^{20}$ Pa s. On the other hand, it is more likely that compaction in such a situation occurs via pressure solution (Angevine and Turcotte, 1983; Birchwood and Turcotte, 1994; Fowler and Yang, 1999). For a one kilometre diameter chamber, the crystallisation time is $\sim d^2/\kappa$ (d is diameter and κ is thermal diffusivity), and this is also 30,000 y. Further exploration of the possible dynamics of an underpressured chamber is beyond the scope of this paper.

5. Conclusions

Although the inevitable complexity of two-phase flows makes for a daunting technical description, the principal conclusions of this paper are fairly simply stated. We have presented a fully coherent model of two-phase flow, and applied it to describe the buoyancy driven counter-current convection which is thought to occur in Strombolian volcanic conduits. Bubbly flow is essentially homogeneous, and can be described by a counter-current flow in which the viscous stresses balance the buoyancy, and this balance leads to a pressure gradient which is less than magmastatic. But it is unlikely that bubbly counter-current flow normally occurs, unless the chamber is very deep, and instead there would be a transition to churn flow, in which the bubbly liquid flow is punctuated by large Taylor bubbles, which move through the liquid. A model for such a flow (52) is even more complicated than that for bubbly flow, but is in fact easier to analyse, and again the pressure gradient in the conduit balances the weight of the fluid mixture, and is therefore significantly less than magmastatic. These conclusions concerning the pressure gradient appear to be robust. Having said that, it must be emphasised that, while the present two-phase flow model incorporates greater realism than earlier two-liquid models, by including the effects of exsolution, it still falls short of a complete description of the conduit flow: the effects of crystals and crystallisation in the flow are not considered, the confounding effects of a more tortuous geometry are ignored, and even within the two-phase flow model itself, very little is known in practice about the controls on flow régimes and the transition between them.

For both types of flow, the magma is significantly underpressured with respect to (pure liquid) magmastatic pressure, and this implies that the chamber pressure is absurdly low. This is a direct consequence of the fact that in scaling the momentum equations for both counter-current and churn flow, the principal resistance opposing the pressure gradient is the buoyancy term: the effects of wall friction and/or interfacial drag are small. While many details of the modelling can be questioned, it seems difficult to find an alternative to this fundamental finding. If this is correct, it raises the issue of how the dynamics of the magma chamber can act in such a way as to maintain the exchange flow for periods of millennia, and a plausible and indeed inevitable suggestion is that the magma chamber acts more like a late-stage crystallising mush. In this view, Strombolian volcanoes would represent a late stage of evolution in the eruptive type of volcanoes.

Acknowledgements

A. C. F. acknowledges the support of the Mathematics Applications Consortium for Science and Industry (www.macsi.ul.ie) funded by the Science Foundation Ireland mathematics grant 12/1A/1683.

Appendix A. Thermal boundary layer

The upwelling and downwelling flows are at temperatures $\theta = 1$ and $\theta = 0$, respectively. Separating the two zones will be a thin boundary layer where the temperature changes rapidly in the neighborhood of $x = s^*$, where $s^* < s$ is the position where $w = 0$ (since $W_d > 0$). For simplicity (only), we consider the case where the upflow $w(x)$ is as in Eq. (32), but $u = 0$ (the extension to the case where also $u \neq 0$ is straightforward). The energy Eq. $(28)_3$ is then

$$Gw\theta_z = \frac{1}{Pr}\theta_{xx}. \tag{87}$$

In the boundary layer we introduce a scaled coordinate X defined by

$$x = s^* + \delta_T X, \tag{88}$$

where δ_T is the width of the layer, and approximate the velocity by

$$w \approx -\Sigma(x - s^*), \quad \Sigma = -w_x(s^*) > 0; \tag{89}$$

Σ depends on α and s, and thus is a function of z. Choosing

$$\delta_T = \left(\frac{1}{GPr}\right)^{1/3} \ll 1, \tag{90}$$

the energy equation becomes

$$-\Sigma X\theta_z = \theta_{XX}. \tag{91}$$

Finally, it remains to prescribe suitable boundary conditions for Eq. (91). To match the interior and outer solutions we prescribe the matching boundary conditions

$$\begin{aligned} &\theta \to 0 \quad \text{as} \quad X \to +\infty, \\ &\theta \to 1 \quad \text{as} \quad X \to -\infty. \end{aligned} \tag{92}$$

We also have the vertical boundary conditions

$$\begin{aligned} &\theta = 1 \quad \text{on} \quad z = 0, \quad X < 0, \\ &\theta = 0 \quad \text{on} \quad z = 1, \quad X > 0. \end{aligned} \tag{93}$$

Eq. (91) together with the boundary conditions (92) and (93) represent the thermal boundary layer problem. The structure of the boundary layer is shown in Fig. 9.

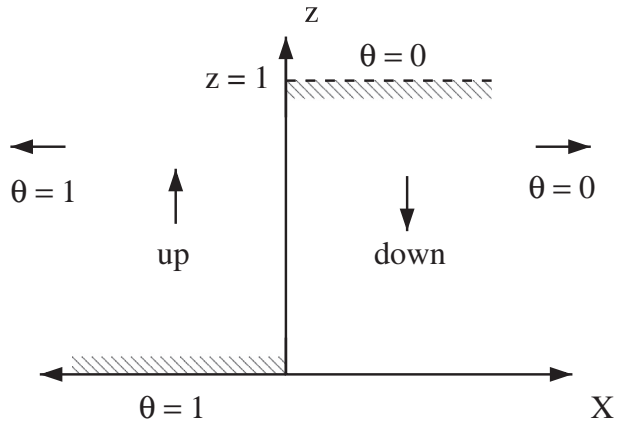

Fig. 9. Structure of the thermal boundary layer.

A.1. Solution of the boundary layer problem

A similar problem to that given by Eqs. (91)–(93) was solved by Howard and Veronis (1987) in the analysis of salt fingers and we briefly describe their method of solution in this section. We will take Σ to be constant for convenience (variable Σ is easily incorporated by a transformation of z). To start, we define

$$\xi = \Sigma^{\frac{1}{3}} X, \tag{94}$$

thus obtaining

$$-\xi\theta_z = \theta_{\xi\xi}, \tag{95}$$

with boundary conditions

$$\begin{aligned} &\theta = 1 \quad \text{when} \quad \xi < 0, \quad z = 0 \quad \text{and} \quad \text{as} \quad \xi \to -\infty, \\ &\theta = 0 \quad \text{when} \quad \xi > 0, \quad z = 1 \quad \text{and} \quad \text{as} \quad \xi \to +\infty. \end{aligned} \tag{96}$$

To solve this, we define

$$\theta(0, z) = \phi(z), \quad \theta_\xi(0, z) = \psi(z). \tag{97}$$

Eq. (91) is solved by Laplace transform in z in the two separate regions $X > 0$ and $X < 0$, using the (unknown) value of ϕ. ψ can then be computed as a convolution integral of ϕ. This can be done in both regions, and elimination of ϕ then yields the integral equation

$$-\frac{1}{3^{\frac{1}{3}}\Gamma\left(\frac{2}{3}\right)} \int_0^1 \frac{\psi(\tau)}{|z - \tau|^{\frac{2}{3}}}\, d\tau = 1, \tag{98}$$

of which the solution is (Howard and Veronis, 1987; Carrier et al., 1966)

$$\psi(z) = -\frac{3^{\frac{1}{3}}\Gamma\left(\frac{2}{3}\right)[z(1 - z)]^{-\frac{1}{6}}}{2\pi}, \tag{99}$$

and then

$$\phi(z) = 1 - \int_0^z \frac{[\tau(1 - \tau)]^{-\frac{1}{6}}}{2\pi(z - \tau)^{\frac{2}{3}}} d\tau. \tag{100}$$

We plot $\phi(z)$ in Fig. 10; solutions for θ at fixed z are shown in Fig. 11.

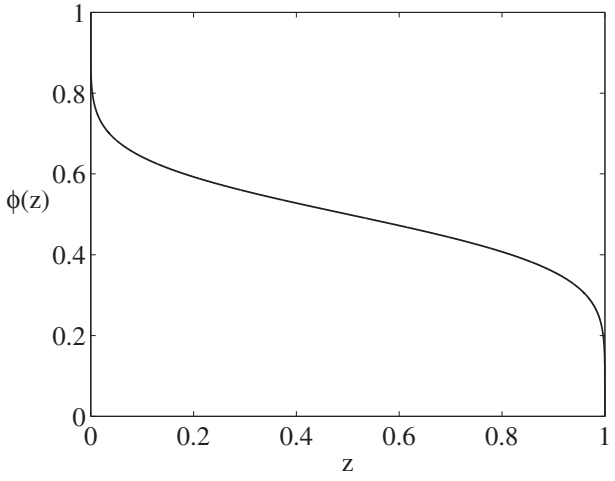

Fig. 10. $\phi(z)$, temperature profile at $\xi = 0$.

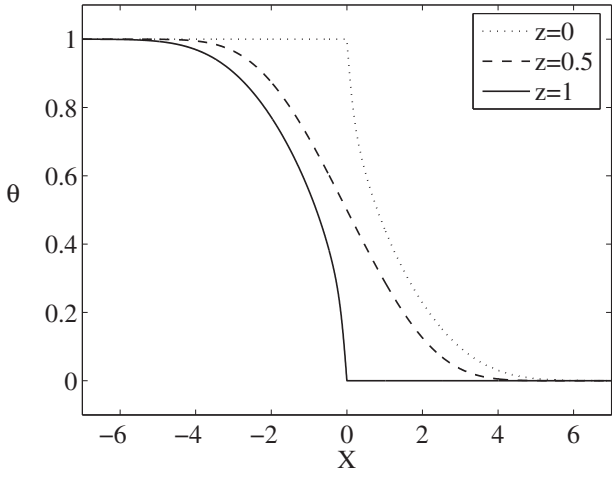

Fig. 11. $\theta(X)$ at fixed values of z.

References

Angevine, C.L., Turcotte, D.L., 1983. Porosity reduction by pressure solution: a theoretical model for quartz arenites. Geol. Soc. Am. Bull. 9, 1,129–1,134.

Barmin, A., Melnik, O., Sparks, R.S.J., 2002. Periodic behaviour in lava dome eruptions. Earth Planet. Sci. Lett. 199, 173–184.

Batchelor, G.K., 1967. An Introduction to Fluid Dynamics. C. U. P., Cambridge.

Beckett, F.M., Burton, M., Mader, H.M., Phillips, J.C., Polacci, M., Rust, A.C., Witham, F., 2014. Conduit convection driving persistent degassing at basaltic volcanoes. J. Volcanol. Geotherm. Res. 283, 19–35.

Beckett, F.M., Mader, H.M., Phillips, J.C., Rust, A.C., Witham, F., 2011. An experimental study of low Reynolds number exchange flow of two Newtonian fluids in a vertical pipe. J. Fluid Mech. 682, 652–670.

Benilov, E.S., Cummins, C.P., Lee, W.T., 2013. Why do bubbles in Guinness sink? Amer. J. Phys. 81, 88–91.

Bercovici, D., Michaut, C., 2010. Two-phase dynamics of volcanic eruption: compaction, compression and the conditions for choking. Geophys. J. Int. 182, 843–864.

Birchwood, R.A., Turcotte, D.L., 1994. A unified approach to geopressuring, low-permeability zone formation, and secondary porosity generation in sedimentary basins. J. Geophys. Res. 99, 20,051–20,058.

Blake, S., 1981. Volcanism and the dynamics of open magma chambers. Nature 289, 783–785.

Burton, M.R., Mader, H.M., Polacci, M., 2007. The role of gas percolation in quiescent degassing of persistently active basaltic volcanoes. Earth Planet. Sci. Lett. 264, 46–60.

Carbone, D., Zuccarello, L., Montalto, P., Rymer, H., 2012. New geophysical insight into the dynamics of Stromboli volcano (Italy). Gondwana Res. 22, 290–299.

Carrier, G.F., Krook, M., Pearson, C.E., 1966. Functions of a Complex Variable: Theory and Technique. McGraw-Hill, New York.

Carrigan, C.R., 1983. A heat pipe model for vertical magma-filled conduits. J. Volcanol. Geotherm. Res. 16, 279–298.

Cashman, K.V., Giordano, G., 2014. Calderas and magma reservoirs. J. Volcanol. Geotherm. Res. 288, 28–45.

Chen, J., Yang, N., Ge, W., Li, J., 2009. Computational fluid dynamics simulation of regime transition in bubble columns incorporating the dual-bubble-size model. Ind. Chem. Res. 48, 8,172–8,179.

Drew, D.A., Passman, S.L., 1999. Theory of Multicomponent Fluids. Springer-Verlag, New York.

Ergun, S., Orning, A.A., 1949. Fluid flow through randomly packed columns and fluidized beds. Ind. Eng. Chem. 41, 1,179–1,184.

Fowler, A., 2011. Mathematical Geoscience. Springer-Verlag, London.

Fowler, A.C., Yang, X.-S., 1999. Pressure solution and viscous compaction in sedimentary basins. J. Geophys. Res. 104, 12,989–12,997.

Fowler, A.C., 1985. A mathematical model of magma transport in the asthenosphere. Geophys. Astrophys. Fluid Dyn. 33, 63–96.

Gonnermann, H.M., Manga, M., 2012. Dynamics of magma ascent in the volcanic conduit. In: Fagents, S.A., Gregg, T.K.P., Lopes, R.M.C. (Eds.), Modeling Volcanic Processes: the Physics and Mathematics of Volcanism. C.U.P., Cambridge, pp. 55–84.

Harris, A.J.L., Stevenson, D.S., 1997. Thermal observations of degassing open conduits and fumaroles at Stromboli and Vulcano using remotely sensed data. J. Volcanol. Geotherm. Res. 76, 175–198.

Hetsroni, G. (Ed.), 1982. Handbook of multiphase systems. Hemisphere, Washington, D.C.

Hewitt, G.F., Roberts, D.N., 1969. Studies of two-phase flow patterns by simultaneous flash and X-ray photography. AERE-M2159, Harwell,

Howard, L.N., Veronis, G., 1987. The salt-finger zone. J. Fluid Mech. 183, 1–23.

Huppert, H.E., Hallworth, M.A., 2007. Bi-directional flows in constrained systems. J. Fluid Mech. 578, 95–112.

Huppert, H.E., Woods, A.W., 2002. The role of volatiles in magma chamber dynamics. Nature 420, 493–495.

Ilanko, T., Oppenheimer, C., Burgisser, A., Kyle, P., 2015. Cyclic degassing of Erebus volcano. Antarct. Bull. Volcanol. 77, 56.

Ishii, M., Zuber, N., 1979. Drag coefficient and relative velocity in bubbly, droplet or particulate flows. AIChE J. 25, 843–855.

James, M.R., Lane, S.J., Corder, S.B., 2008. Modelling the rapid near-surface expansion of gas slugs in low-viscosity magmas. Geol. Soc. Lond. Spec. Publ. 307, 147–167.

James, M.R., Lane, S.J., Houghton, B.F., 2013. Unsteady explosive activity: Strombolian eruptions. In: Fagents, S.A., Gregg, T.K.P., Lopes, R. M. C (Eds.), Modeling Volcanic Processes: the Physics and Mathematics of Volcanism. C. U. P., Cambridge, pp. 107–128.

Jaupart, C., Vergniolle, S., 1988. Laboratory models of Hawaiian and Strombolian eruptions. Nature 331, 58–60.

Jaupart, C., Vergniolle, S., 1989. The generation and collapse of a foam layer at the roof of a basaltic magma chamber. J. Fluid Mech. 203, 347–380.

Kazahaya, K., Shinohara, H., Saito, G., 1994. Excessive degassing of Izu-Oshima volcano: magma convection in a conduit. Bull. Volcanol. 56, 207–216.

Kazahaya, K., Shinohara, H., Saito, G., 2002. Degassing process of Satsuma-Iwojima volcano, Japan: supply of volatile components from a deep magma chamber. Earth Planets Space 54, 327–335.

Mangan, M., Mastin, L., Sisson, T., 2004. Gas evolution in eruptive conduits: combining insights from high temperature and pressure decompression experiments with steady-state flow modeling. J. Volcanol. Geotherm. Res. 129, 23–36.

Mangan, M., Sisson, T., 2005. Evolution of melt-vapor surface tension in silicic volcanic systems: experiments with hydrous melts. J. Geophys. Res. 110, B01202.

Massol, H., Jaupart, C., 1999. The generation of gas overpressure in volcanic eruptions. Earth Planet. Sci. Lett. 166, 57–70.

McKenzie, D., 2011. Compaction and crystallization in magma chambers: towards a model of the Skaergaard intrusion. J. Petrol. 52, 905–930.

Melnik, O., 2000. Dynamics of two-phase conduit flow of high-viscosity gas-saturated magma: large variations of sustained explosive eruption intensity. Bull. Volcanol. 62, 153–170.

Melnik, O., Sparks, R.S.J., 1999. Nonlinear dynamics of lava extrusion. Nature 402, 37–41.

Melnik, O., Sparks, R.S.J., 2002. Dynamics of magma ascent and lava extrusion at the Soufrière Hills Volcano, Montserrat. In: Druitt, T.H., Kokelaar, B.P. (Eds.), The Eruption of the Soufrière Hills Volcano, Montserrat, 1995 to 1999. Geol. Soc. Lond. Mem. 21. pp. 153–172.

Métrich, N., Bertagnini, A., Landi, P., Rosi, M., 2001. Crystallization driven by decompression and water loss at Stromboli volcano (Aeolian Islands, Italy). J. Petrol. 42, 1,471–1,490.

Métrich, N., Bertagnini, A., di Muro, A., 2010. Conditions of magma storage, degassing and ascent at Stromboli: new insights into the volcano plumbing system with inferences on the eruptive dynamics. J. Petrol. 51, 603–626.

Molina, I., Burgisser, A., Oppenheimer, C., 2012. Numerical simulations of convection in crystal-bearing magmas: a case study of the magmatic system at Erebus, Antarctica. J. Geophys. Res. 117, B07209.

Montoya, G., Lucas, D., Baglietto, E., Liao, Y., 2016. A review on mechanisms and models for the churn-turbulent flow regime. Chem. Eng. Sci. 141, 86–103.

Moussallam, Y., Oppenheimer, C., Scaillet, B., Buisman, I., Kimball, C., Dunbar, N., Burgisser, A., Schipper, C.I., Andújar, J., 2015. Megacrystals track magma convection between reservoir and surface. Earth Planet. Sci. Lett. 413, 1–12.

Palma, J.L., Blake, S., Calder, E.S., 2011. Constraints on the rates of degassing and convection in basaltic open vent volcanoes. Geochem. Geophys. Geosyst. 12 (11), Q11006.

Parfitt, L., Wilson, L., 2008. Fundamentals of Physical Volcanology. Wiley-Blackwell.

Pioli, L., Bonadonna, C., Azzopardi, B.J., Philips, J.C., Ripepe, M., 2012. Experimental constraints on the outgassing dynamics of basaltic magmas. J. Geophys. Res. 117, B03204.

Princen, H.M., Kiss, A.D., 1989. Rheology of foams and highly concentrated emulsions. IV. An experimental study of the shear viscosity and yield stress of concentrated emulsions. J. Colloid Interface Sci. 128, 176–187.

Rust, A.C., Cashman, K.V., 2011. Permeability controls on expansion and size distributions of pyroclasts. J. Geophys. Res. 116, B11202.

Shinohara, H., Kazahaya, K., Lowenstern, J.B., 1995. Volatile transport in a convection magma column: implications for porphyry Mo mineralization. Geology 23, 1091–1094.

Slezin, Y.B., 2003. The mechanism of volcanic eruption (steady state approach). J. Volcanol. Geotherm. Res. 122, 7–50.

Sparks, R.S.J., 2003. Dynamics of magma degassing. In: Oppenheimer, C., Pyle, D.M., Barclay, J. (Eds.), Volcanic Degassing. Geol. Soc. Lond. Spec. Publ. 213. pp. 5–22.

Starostin, A.B., Barmin, A.A., Melnik, O.E., 2005. A transient model for explosive and phreatomagmatic eruptions. J. Volcanol. Geotherm. Res. 143, 133–151.

Stevenson, D.S., Blake, S., 1998. Modelling the dynamics and thermodynamics of volcanic degassing. Bull. Volcanol. 60, 307–317.

Stix, J., 2007. Stability and instability of quiescently active volcanoes: the case of Masaya, Nicaragua. Geology 35, 535–538.

Suckale, J., Keller, T., Cashman, K.V., Persson, P.-O., 2016. Flow-to-fracture transition in a volcanic mush plug may govern normal eruptions at Stromboli. Geophys. Res. Lett. 43, 12,071–12,081.

Tait, S., Jaupart, C., Vergniolle, S., 1989. Pressure, gas content and eruption periodicity of a shallow, crystallising magma chamber. Earth Planet. Sci. Lett. 92, 107–123.

Vergniolle, S., Gaudemer, Y., 2015. From reservoirs and conduits to the surface: review of role of bubbles in driving basaltic eruptions. In: Carey, R., Cayol, V., Poland, M., Weis, D. (Eds.), Hawaiian Volcanoes: From Source to Surface. AGU Geophysical Monograph 208. pp. 289–321.

Vergniolle, S., Jaupart, C., 1986. Separated two-phase flow in basaltic eruptions. J. Geophys. Res. 91, 12,840–12,860.

Vergniolle, S., Jaupart, C., 1990. Dynamics of degassing at Kilauea volcano, Hawaii. J. Geophys. Res. 95, 2,793–2,809.

Vergniolle, S., Mangan, M., 2000. Hawaiian and Strombolian eruptions. In: Sigurdsson, H. (Ed.), Encyclopedia of volcanoes. Academic Press, San Diego, pp. 447–461.

Voight, B., Sparks, R.S.J., Miller, A.D., Stewart, R.C., Hoblitt, R.P., Clarke, A., Ewart, J., Aspinall, W.P., Baptie, B., Calder, E.S., Cole, P., Druitt, T.H., Hartford, C., Herd, R.A., Jackson, P., Lejeune, A.M., Lockhart, A.B., Loughlin, S.C., Luckett, R., Lynch, L., Norton, G.E., Robertson, R., Watson, I.M., Watts, R., Young, S.R., 1999. Magma flow instability and cyclic activity at Soufrière Hills Volcano, Montserrat, British West Indies. Science 283, 1,138–1,142.

Wadsworth, F.B., Kennedy, B.M., Branney, M.J., von Aulock, F.W., Lavallée, Y., Menendez, A., 2015. Exhumed conduit records magma ascent and drain-back during a Strombolian eruption at Tongariro volcano, New Zealand. Bull. Volcanol. 77, 71.

Wallis, G.B., 1969. One-Dimensional Two-Phase Flow. McGraw-Hill, New York.

Witham, F., 2011. Conduit convection, magma mixing, and melt inclusion trends at persistently degassing volcanoes. Earth Planet. Sci. Lett. 301, 345–352.

Witham, F., Llewellin, E.W., 2006. Stability of lava lakes. J. Volcanol. Geotherm. Res. 158, 321–332.

Witter, J.B., Kress, V.C., Delmelle, P., Stix, J., 2004. Volatile degassing petrology and magma dynamics of the Villarica lava lake, Southern Chile. J. Volcanol. Geotherm. Res. 134, 303–337.

Wu, M.-S., Sullivan, M.E., Yee, D.J., 1984. The viscosity of a foam (air in water emulsion). Colloids Surf. 12, 375–380.